

**PHOTOCATALYTIC SEAWATER  
DESALINATION: THE EFFECT OF METAL  
LOADING IN THE HYBRID  $\text{TiO}_2$  AND THE  
EFFECT OF WAVELENGTH**

**AFIQ HAFIZI BIN AZIZI**

**BACHELOR OF CHEMICAL ENGINEERING  
UNIVERSITI MALAYSIA PAHANG**

©AFIQ HAFIZI BIN AZIZI (2015)

## Thesis Access Form

No \_\_\_\_\_ Location \_\_\_\_\_

Author : .....

Title : .....

Status of access OPEN / RESTRICTED / CONFIDENTIAL

Moratorium period: \_\_\_\_\_ years, ending \_\_\_\_\_ / \_\_\_\_\_ 20 \_\_\_\_\_

Conditions of access proved by (CAPITALS): **DR RUZINAH BINTI ISHA**

Supervisor (Signature).....

Faculty: .....

Author's Declaration: *I agree the following conditions:*

OPEN access work shall be made available in the Universiti Malaysia Pahang only and not allowed to reproduce for any purposes.

*The statement itself shall apply to ALL copies:*

**This copy has been supplied on the understanding that it is copyright material and that no quotation from the thesis may be published without proper acknowledgement.**

**Restricted/confidential work:** All access and any photocopying shall be strictly subject to written permission from the University Head of Department and any external sponsor, if any.

**Author's signature**.....Date: .....

users declaration: for signature during any Moratorium period (Not Open work):

***I undertake to uphold the above conditions:***

Date	Name (CAPITALS)	Signature	Address

**PHOTOCATALYTIC SEAWATER  
DESALINATION: THE EFFECT OF METAL  
LOADING IN THE HYBRID TiO<sub>2</sub> AND THE  
EFFECT OF WAVELENGTH**

**AFIQ HAFIZI BIN AZIZI**

Thesis submitted in partial fulfilment of the requirements  
for the award of the degree of  
Bachelor of Chemical Engineering

**Faculty of Chemical & Natural Resources Engineering  
UNIVERSITI MALAYSIA PAHANG**

JULY 2015

©AFIQ HAFIZI BIN AZIZI (2015)

## **SUPERVISOR'S DECLARATION**

We hereby declare that we have checked this thesis and in our opinion, this thesis is adequate in terms of scope and quality for the award of the degree of Bachelor of Chemical Engineering.

Signature :  
Name of main supervisor : DR. RUZINAH BINTI ISHA  
Position :  
Date :

## **STUDENT'S DECLARATION**

I hereby declare that the work in this thesis is my own except for quotations and summaries which have been duly acknowledged. The thesis has not been accepted for any degree and is not concurrently submitted for award of other degree.

Signature :  
Name : AFIQ HAFIZI BIN AZIZI  
ID Number : KA11061  
Date :

*Dedication*

*Dedicated to*

*My parents;*

*Azizi Bin Baharudin*

*Norazizah Binti Ahmad Taif*

*My sisters;*

*Nur Aqilah Binti Azizi*

*My brother;*

*Muhammad Haziq Bin Azizi*

*And*

*My supervisor;*

*Dr. Ruzinah Binti Isha*

*For being supportive*

## **ACKNOWLEDGEMENT**

Praise to Allah for His help and guidance that we finally able to complete this undergraduate research project.

Here, my sincerest gratitude is awarded to my supervisor, Dr Ruzinah Binti Isha for her valuable guidance, advices, constant support and her valuable time towards finishing the final year project. Following her guidance, I am able to understand more about the project. I am very thankful and indebted with her for all her cooperation, tolerance and commitment in assisting me to make this project success and supported me to be a good proposal and thesis writer.

Special thanks also heading to my friends who always give me good advice and always support me. They are also very supportive and always assists me in various occasions. Last but not least, I want to thank to my and parents for supporting me in part of physical and mental and also to all who had assisted and making this project success.

Thank You.

## ABSTRACT

Hybrid photocatalyst of Titanium Dioxide ( $\text{TiO}_2$ ) and biomass ash catalyst become an attractive alternative promoter for seawater desalination. The effect of metal loading in the seawater desalination via photocatalytic reaction at different wavelength light source was investigated. The hybrid catalyst with different weight ratio of  $\text{TiO}_2$ , Oil palm fiber ash and metal loading either Nickel or Ferum was synthesized via wet impregnation. The catalysts were then characterized by using Scanning Electron Microscopy (SEM), Brunauer Emmett Teller (BET), X-ray Diffraction (XRD). The natural seawater were analysed for its pH, conductivity, turbidity, Biochemical Oxygen Demand (BOD) and Chemical Oxygen Demand (COD) prior the experiment. Then the catalyst was tested with the natural seawater using photocatalytic reactor with the weight ratio of 1:400 catalyst and seawater. The experiment was conducted for two hours in a mercury light exposure with the wavelength of 365 nm and 420 nm respectively. The pH, conductivity, turbidity, BOD and COD of the final product were analysed. It is found that there was an increment of the seawater quality in term of salt concentration, COD and BOD. By using 365 nm wavelength light and nickel loading catalyst, the salt concentration, COD and BOD reduced up to 4%, 88%, and 68% respectively. Meanwhile, the reduction of COD and BOD were achieved at 95% and 97% when 420 nm wavelength light and ferum loading catalyst were used. At 420 nm wave length, the salt concentration was increasing due to the distillation. It because at 420 nm wavelength the water was heated up to 100 °C and causing the distillation to dominates the process. Nickel loading catalyst perform at best when 365 nm light was used, while ferum loading work great when 420 nm light was used. It is because the performance of the metal loading was due to the different characterization of the metal band gap in which the smaller the band gap, the bigger the wavelength. Nickel has bigger band gap than ferum. It can be concluded that the addition of the metal loading improve the performance of the catalyst due to the different band characterization of the metal loading and changes of wavelength can affect the performance of the catalyst.

## **ABSTRAK**

Fotomangkin hibrid Titanium Dioksida ( $\text{TiO}_2$ ) dan pemangkin abu biomas menjadi promoter alternatif menarik bagi penyahmasinan air laut. Kesan pembebanan logam di penyahgaraman air laut melalui reaksi fotopemangkinan pada sumber cahaya yang berbeza panjang gelombang dikaji. Pemangkin hibrid dengan nisbah yang berbeza berat  $\text{TiO}_2$ , abu serat kelapa sawit dan muatan logam sama ada Nikel atau Ferum telah disintesis melalui pengisitepuan basah. Pemangkin kemudian dicirikan dengan menggunakan Scanning Electron Microscopy (SEM), Brunauer Emmett Teller (BET), X-ray Diffraction (XRD). Air laut semula jadi dianalisis untuk yang pH, kekonduksian, kekeruhan, Keperluan Oksigen Biokimia (BOD) dan Permintaan Oksigen Kimia (COD) sebelum percubaan. Kemudian pemangkin diuji dengan air laut yang semula jadi dengan menggunakan reaktor fotopemangkinan dengan nisbah berat 1: 400 pemangkin dan air laut. Eksperimen ini dijalankan selama dua jam dalam pendedahan cahaya merkuri dengan panjang gelombang 365 nm dan 420 nm masing-masing. pH, kekonduksian, kekeruhan, BOD dan COD produk akhir telah dianalisis. Didapati bahawa terdapat peningkatan kualiti air laut dari segi kepekatan garam, COD dan BOD. Dengan menggunakan 365 nm panjang gelombang cahaya dan nikel mangkin, kepekatan garam, COD dan BOD dikurangkan sehingga masing-masing kepada 4 %, 88 %, dan 68 %. Sementara itu, pengurangan COD dan BOD telah dicapai pada 95 % dan 97 % apabila 420 nm cahaya panjang gelombang dan ferum mangkin digunakan. Pada 420 nm panjang gelombang, kepekatan garam yang semakin meningkat disebabkan oleh penyulingan. Ia kerana pada 420 nm panjang gelombang, air telah dipanaskan sehingga 100 °C dan menyebabkan penyulingan untuk menguasai proses. Nikel loading prestasi terbaik apabila 365 nm cahaya telah digunakan, manakala prestasi terbaik ferum loading apabila 420 nm cahaya telah digunakan. Ia adalah kerana prestasi loading besi ini bergantung pada perwatakan yang berbeza daripada jurang jalur logam di mana lebih kecil jurang ini, semakin besar panjang gelombang. Nikel mempunyai jurang jalur lebih besar daripada ferum. Ia boleh membuat kesimpulan bahawa penambahan muatan logam meningkatkan prestasi pemangkin kerana pencirian yang berbeza muatan logam dan perubahan panjang gelombang boleh mengubah prestasi pemangkin.

# TABLE OF CONTENTS

SUPERVISOR'S DECLARATION .....	V
STUDENT'S DECLARATION .....	VI
<i>Dedication</i> .....	VII
ACKNOWLEDGEMENT .....	VIII
ABSTRACT.....	IX
ABSTRAK.....	X
TABLE OF CONTENTS.....	XI
LIST OF FIGURES .....	XIII
LIST OF TABLES .....	XV
LIST OF ABBREVIATIONS.....	XVI
1 INTRODUCTION.....	1
1.1 Research Background .....	1
1.2 Motivation and statement of problem .....	2
1.3 Objectives.....	4
1.4 Scope of this research .....	4
2 LITERATURE REVIEW .....	5
2.1 Introduction.....	5
2.2 Photocatalytic process.....	5
2.3 Photocatalytic Reactor .....	6
2.4 Titanium Dioxide (TiO <sub>2</sub> ).....	7
2.5 Mechanism of Photocatalytic Reaction.....	7
2.6 Oil palm fiber ash (Biomass Ash).....	9
2.7 Metal Loading in Photocatalyst .....	10
3 MATERIALS AND METHODS .....	11
3.1 Introduction.....	11
3.2 Material .....	12
3.2.1 Natural Seawater (NSW).....	12
The NSW sample from Teluk Cempedak Kuantan, Pahang. The sample was stored at 4 °C in the refrigerator. ....	12
3.2.2 Oil palm fiber ash (Biomass ash) .....	12
3.2.3 Chemical.....	12
3.3 Preparation of Solution and Catalyst .....	12
3.3.1 Preparation of NSW .....	12
3.3.2 Preparation of Catalyst .....	13
3.3.3 Characterization of Catalyst .....	13
3.4 Photocatalytic Reactor Set Up .....	15
3.5 Experimental Procedure.....	16
3.6 Analytical Test .....	16
3.6.1 pH, Conductivity and Total Dissolved Solid (TDS) .....	16
3.6.2 Chemical Oxygen Demand (COD) .....	17
3.6.3 Biochemical Oxygen Demand (BOD) .....	18
4 RESULT AND DISCUSSION.....	19
4.1 Introduction.....	19
4.2 Property of Seawater Sample.....	19
4.3 The Effect of Metal Loading.....	20

4.4	The Effect of Wavelength .....	27
4.4.1	No Metal Loading .....	28
4.4.2	Nickel Loading .....	34
4.4.3	Ferum Loading .....	40
4.4.4	SEM Characterization .....	46
4.4.5	Summary .....	47
5	CONCLUSION AND RECOMMENDATION .....	49
5.1	Conclusion .....	49
5.2	Recommendation .....	50
	References.....	51
	APPENDICES .....	55

## LIST OF FIGURES

Figure 3-1: Flow diagram of experimental procedure. ....	11
Figure 3-2: Scanning Electron Microscopy (SEM). ....	14
Figure 3-3: Brunauer Emmett Teller (BET). ....	14
Figure 3-4: X-Ray Diffraction (XRD). ....	15
Figure 3-5: The schematic diagram of photocatalytic reactor .....	15
Figure 3-6: pH, conductivity and TDS meter. ....	17
Figure 3-7: COD measuring equipment (a) COD digestion reactor (b) COD spectrophotometer.....	17
Figure 3-8: Dissolved oxygen meter.....	18
Figure 4-1: SEM image of the fresh catalyst: a) no metal b) with nickel loading c) with ferum loading .....	20
Figure 4-2: Percentage of reduction for the NSW analysis. ....	21
Figure 4-3: Percentage of reduction for the conductivity of NSW analysis. ....	22
Figure 4-4: Percentage of reduction for the TDS of NSW analysis. ....	23
Figure 4-5: XRD analysis for the metal loading catalyst.....	23
Figure 4-6: Percentage of reduction for the BOD of NSW analysis. ....	25
Figure 4-7: Percentage of reduction for the COD of NSW analysis. ....	26
Figure 4-8: SEM image of the used catalyst: (a) fresh no metal loading (b) used no metal loading (c)fresh nickel loading (d) used nickel loading (e) fresh ferum loading (f) used ferum loading.....	27
Figure 4-9: NSW analysis for pH. ....	29
Figure 4-10: Percentage of reduction for pH. ....	29
Figure 4-11: NSW analysis for conductivity. ....	30
Figure 4-12: NSW analysis for TDS.....	30
Figure 4-13: XRD analysis (a) 365 nm (b) 420 nm.....	31
Figure 4-14: NSW analysis for BOD.....	32
Figure 4-15: Percentage of reduction for BOD. ....	33
Figure 4-16: NSW analysis for COD.....	33
Figure 4-17: Percentage of reduction for COD. ....	34
Figure 4-18: NSW analysis for pH. ....	35
Figure 4-19: Percentage of reduction for pH. ....	35
Figure 4-20: NSW analysis for conductivity. ....	36
Figure 4-21: NSW analysis for TDS.....	36
Figure 4-22: XRD analysis (a) 365 nm (b) 420 nm.....	37

Figure 4-23: NSW analysis for BOD.....	38
Figure 4-24: Percentage of reduction for BOD. ....	39
Figure 4-25: NSW analysis for COD.....	39
Figure 4-26: Percentage of reduction for COD. ....	40
Figure 4-27: NSW analysis for pH. ....	41
Figure 4-28: NSW analysis for conductivity. ....	42
Figure 4-29: NSW analysis for TDS.....	42
Figure 4-30: XRD analysis (a) 365 nm (b) 420 nm.....	43
Figure 4-31: NSW analysis for BOD.....	44
Figure 4-32: Percentage of reduction for BOD. ....	45
Figure 4-33: NSW analysis for COD.....	45
Figure 4-34: Percentage of reduction for COD. ....	46
Figure 4-35: SEM image of the used catalyst: (a) fresh no metal loading (b) used no metal loading (c)fresh nickel loading (d) used nickel loading (e) fresh ferum loading (f) used ferum loading.....	47
Figure 4-36 : The overall comparison for the percentage of reduction for 365 nm and 420 nm wavelength light.....	48

## LIST OF TABLES

Table 2-1: General mechanism of the photocatalytic reaction on illuminated TiO <sub>2</sub> (Teh & Mohamed 2011).....	8
Table 2-2: The research on utilization of fly ash.....	9
Table 2-3: The research on effect of metal in photocatalyst.....	10
Table 3-1: The weight ratio of the three catalyst.....	13
Table 4-1: Fresh NSW analysis .....	19
Table 4-2: NSW analysis after the photocatalytic reaction.....	21
Table 4-3: BET analysis for the metal loading catalyst.....	24
Table 4-4: NSW analysis after the photocatalytic reaction at 420 nm.....	28
Table 4-5: NSW analysis for no metal loading catalyst.....	28
Table 4-6: BET analysis for no metal loading catalyst.....	31
Table 4-7: NSW analysis for nickel loading catalyst.....	34
Table 4-8: BET analysis for no metal loading catalyst.....	37
Table 4-9: NSW analysis for nickel loading catalyst.....	41
Table 4-10: BET analysis for ferum loading catalyst.....	43

## LIST OF ABBREVIATIONS

TiO <sub>2</sub>	Titanium dioxide
COD	Chemical Oxygen Demand
BOD	Biochemical Oxygen Demand
SEM	Scanning Electron Microscopy
BET	Brunnauer Emmett Teller
XRD	X-ray Diffraction
NSW	Natural seawater
(Ni(NO <sub>3</sub> ) <sub>2</sub> ·6H <sub>2</sub> O)	Nickel Nitrate Hexahydrate
(Fe(NO <sub>3</sub> ) <sub>3</sub> ·9H <sub>2</sub> O)	Ferum Nitrate Hydrate
VB	Valence band
CB	Conduction band
E <sub>bg</sub>	Band gap energy

# 1 INTRODUCTION

## 1.1 Research Background

Water is made out of two hydrogen and one oxygen, it is one of the most essential elements to health and is so important that your body actually has a specific drought management system in place to prevent dehydration and ensure your survival. Water makes up more than two thirds of human body weight, and without water, we would die in a few days. The human brain is made up of 95 % water, blood is 82 % and lungs 90 %. A mere 2 % drop in our body's water supply can trigger signs of dehydration: fuzzy short-term memory, trouble with basic math, and difficulty focusing on smaller print, such as a computer screen. Therefore water is essential to sustain the human life and good clean water accessibility is very importance. These is because good access to clean water will benefit us with good health and prevent hydration of the body. The problem faced nowadays is the water shortag (Shakhashiri, 2011)e problem due to the expanding of world population and the current water source is fresh water where it only covered 1.7 % of the world water. Therefore seawater which cover 96 % of the world water has to use (Wolf, 1999). The country that has started to u (Esplugas, et al., 2002) (Pera-Titus, et al., 2004)se seawater as their main source of water are the Middle East country and Africa. Both country depend on the desalinate seawater to overcome their water shortage problem (Ghaffour, et al., 2011).

The seawater can be desalinate to clean water using several method like distillation (Ghaffour, et al., 2011)where the water is heated at high temperature so that the water evaporates and separated from the salt, electrodialysis where the salt ion is transport from one solution through ion-exchange membranes to another solution under the influence of an applied electric potential difference, and the reverse osmosis (Akili, et al., 2008) (Francois, et al., 2008) method where membrane is used. The method used for desalination of seawater mostly require high energy which will lead to high cost (Shakhashiri, 2011). That is why there still many country that have not use seawater as their main source of water supplies even though seawater cover 96 % of the world water.

The researcher nowadays also, are trying to develop or modified the current technologies for seawater desalination so that the energy and cost consumption can be reduced.

These have led to the study in the field of advanced oxidation process (AOP) as the alternative to the desalination technologies. The rationales of these AOPs are based on the in-situ generation of highly reactive transitory species for mineralization of refractory organic compounds, water pathogens and disinfection by-products (Esplugas, et al., 2002) (Pera-Titus, et al., 2004). Among these AOPs, heterogeneous photocatalysis employing semiconductor catalysts ( $\text{TiO}_2$ ,  $\text{ZnO}$ ,  $\text{Fe}_2\text{O}_3$ ,  $\text{CdS}$ ,  $\text{GaP}$  and  $\text{ZnS}$ ) has demonstrated its efficiency in degrading a wide range of ambiguous refractory organics into readily biodegradable compounds, and eventually mineralized them to innocuous carbon dioxide and water. Among the semiconductor catalysts, titanium dioxide ( $\text{TiO}_2$ ) has received the greatest interest. The  $\text{TiO}_2$  is the most active photocatalyst under the photon energy of  $300 \text{ nm} < \lambda < 390 \text{ nm}$  and remains stable after the repeated catalytic cycles, whereas  $\text{CdS}$  or  $\text{GaP}$  are degraded along to produce toxic products (Malato, et al., 2009). Other than these, the multi-faceted functional properties of  $\text{TiO}_2$  catalyst, such as their chemical and thermal stability or resistance to chemical breakdown and their strong mechanical properties have promoted its wide application in photocatalytic water treatment (Chong, 2010).

For these study, the photocatalytic reaction of the Titanium Dioxide was tested on the seawater in order to see the effectiveness of the reaction to absorb the salt content of the seawater and purification of the seawater. In these study also the Titanium Dioxide was mixed with biomass ash and metal as supported catalyst in order to improve the efficiency and the performance of the catalyst. The catalyst also was tested with different wavelength to see whether the performance of the catalyst increase or decrease due to the different wavelength light.

## **1.2 Motivation and statement of problem**

Water is known as a colourless, transparent, odourless, liquid which forms the seas, lakes, rivers and rain and is the basis fluid of the living organism (Anon., 2014). All form of life need water and human consume drinking water which has qualities with the human body. Ordinary rain water in many countries has been polluted and therefore it is not safe to

drink directly. This natural resource has become scarce with the growing world population, and its availability is a major social and economic concern (Anon., 2004).

Based on the U.S Geological Survey, it is found that 96.5% Earth's water is located in seas and ocean and 1.7% of Earth's water is located in the ice caps. Approximately 0.8% is considered to be fresh water. The remaining is made up of brackish water, slightly salty water found as surface water in estuaries and as ground water in salty aquifers(Gleick 1998). Water shortages have plagued many people and human have long searched for a solution to Earth's lack of fresh water supplies.

Today, the world is concern on the problem related to the production of potable water. This is because the project population growth and demand exceed conventional available water resources. According to Service (2006), over one billion people are living without clean drinking water and approximately 2.3 billion people which is 41% of the world population live in region with water shortages. Besides that, most of the solutions that present nowadays are not sufficient to cope with the increasing demand and decreasing supply. Furthermore, most of the traditional source like the river, lake and ground water is misused and causing them to diminish through time (Greenlee et al. 2009). Therefore, as a solution, human being has to find another alternative to overcome this problem. The solution is the seawater because it is abundant and underutilised.

Israel for instance, when their water balance shows an increasing deficit throughout the years and the other regional demands for their water, their authorities has launched the desalination master plan, compromising a large scale seawater desalination of seawater in order to overcome the problem (Lokiec & Kronenberg 2003). While in China, they have been developing seawater technologies for the past six decades to overcome their water shortage problem especially at their coastal areas (Zheng et al. 2014). Thus, desalination is the best solution for the world water shortage problem but it is estimated that some 30% of the world's areas suffer from salinity problem and the remediation is seen very costly (Anon., 2014). Therefore, another method of purifying the seawater need to be developed.

### **1.3 Objectives**

The objectives of this study are:

- a) to synthesize and characterize the hybrid catalyst of titanium dioxide (TiO<sub>2</sub>) with biomass ash and metal
- b) to study the effect of the metal loading in photocatalytic seawater purifying processes.

### **1.4 Scope of this research**

The scope of this research are:

- a) Rig set up for the photocatalytic reactor is designed and fabricated.
- b) The catalyst with different weight ratio of TiO<sub>2</sub> to palm oil fibre ash to metal loading which are Nickel (Ni) or Ferum (Fe) was synthesized using wet impregnation. The catalyst performance was tested in the photocatalytic reactor with the weight ratio of catalyst to seawater of 1:400 for two hours.
- c) Characterization of the fresh and used catalyst using Scanning Electron Microscopy (SEM), Brunauer Emmet Taller(BET) and X-tray Diffraction(XRD) was done.
- d) The pH, conductivity, turbidity, Chemical Oxygen Demand(COD) and Biochemical Oxygen Demand (BOD) were analysed before and after the experiments

## 2 LITERATURE REVIEW

### 2.1 Introduction

Seawater is becoming an increasingly important water source worldwide, and this study aims to examine the effect of metal loading with TiO<sub>2</sub> in the photocatalytic process for seawater purification. An overall aim is to investigate the capability of photocatalytic treatment of saline waters in minimising dissolved organic matter and salt so that it can be used in daily use municipal water.

### 2.2 Photocatalytic process

In 1972, Fujishima and Honda discovered the photocatalytic reaction of water splitting on TiO<sub>2</sub> electrodes. This discovery marked the beginning of a new era in heterogeneous photocatalysis. Since the discovery, there are many research efforts in understanding the fundamental processes and in enhancing the photocatalytic efficiency of TiO<sub>2</sub> have come from extensive research performed by chemists, physicists, and chemical engineers. Such studies are often related to energy renewal and energy storage but in recent years, the heterogeneous photocatalysis has been involved in applications for environmental cleanup. This is inspired by the potential application of TiO<sub>2</sub>-based photocatalysts for the total destruction of organic compounds in polluted air and wastewater (A. Fujishima, 1999).

The current successful photocatalytic systems for overall water splitting can be divided into two primary approaches. The first approach is to split water into H<sub>2</sub> and O<sub>2</sub> using a single visible-light-responsive photocatalyst with a sufficient potential to achieve overall water splitting. In this system, the photocatalyst should have a suitable thermodynamic potential for water splitting, a sufficiently narrow band gap to harvest visible photons, and stability against photocorrosion. Because of these stringent requirements, the number of reliable, reproducible photocatalysts suitable for one-step water splitting is limited (Maeda, et al., 2005; Lee, et al., 2007). The other approach is to apply a two-step excitation mechanism using two different photocatalysts. This approach was inspired by natural photosynthesis in green plants and is called the Z-scheme. The advantages of a Z-scheme water splitting system are that a wider range of visible light is available because a change in Gibbs free energy required to drive each photocatalyst can be reduced as

compared to the one-step water splitting system and that the separation of evolved H<sub>2</sub> and O<sub>2</sub> is possible. It is also possible to use a semiconductor that has either a water reduction or oxidation potential for one side of the system (Bard, 1979).

### **2.3 Photocatalytic Reactor**

Reactor design is an importance focus for photocatalytic reaction because it is importance to perform the experimental work. The reactor design for the photocatalytic reaction can be divided into two categories which are lab scale where the volume of reactant solution is below one litre (Zhang et.al.2011, Natarajan et.al, 2011) and the pilot scale reactor where the reactor volume is more than five litre (Pereira et.al, 2011, Vilar et.al, 2009). The recent innovation for the lab scale reactor are the use of energy efficient UV/visible light emitting diodes (LEDs) as light sources (Wang et.al, 2010, Nickel et.al, 2012), the design of rotating disc type reactor model (Natarajan et.al, 2011, Chang et.al, 2010), the fabrication of NTO-immobilized catalytic beds (Raoet.al, 2012, Ji et.al, 2011) and post-separation/reuse of nano crystalline Titanium Dioxide (NTO) powder catalysts (Kim et.al, 2010, Suryaman et.al, 2012). LEDs are used because the LEDs is a light sources that need less energy and, therefore, LED-based photocatalytic reactors are more energy-efficient systems. The combination of UV-LEDs and NTO powder (Natarajan, 2011), NTO nanotubes , or immobilized NTO (Nickel et.al, 2012) has been reported for the degradation of various dyes such as methyl orange, methylene blue, rhodamine B, and malachite green. The UV-LED photoreactor design by Nickels *et al.* (2012) was equipped with a microcirculating fluid pump so that the reactant is completely mixed and an in-stream sensor unit. The sensor unit, an assembly of a liquid flow cell with transparent windows, an LED lamp, and a photodiode monitor, are installed so that it enabled the real-time evaluation of the decrease in the concentration of methyl orange dye. The reactor also have other special attribute which are it is light weight, low production cost, and flexibility, make this design ideal for both laboratory and field work applications. Visible LEDs with carbon-nitrogen co-doped NTO achieved the visible light degradation of bisphenol (Wang et.al, 2010). The reactor has of four strips of visible LEDs which covered the wavelength range of 450 to 600 nm.

## 2.4 Titanium Dioxide (TiO<sub>2</sub>)

Starting in the late 1960s, researchers study the application and characteristic of TiO<sub>2</sub>. This story, whose keywords are TiO<sub>2</sub> and light, began with photo electrochemical solar energy conversion, and then shifted into the area of environmental photocatalysis and photo-induced hydrophilicity, and most recently into the commercialization of TiO<sub>2</sub>-based photocatalytic products. (Fujishima, 2005)

Titanium dioxide (n-TiO<sub>2</sub>) was recognized to be the most promising semiconductor. It has been widely used as a catalyst because of its optical and electronic properties, low cost, high level of photocatalytic activity, chemical stability and non-toxicity. Over the past several years, the application of TiO<sub>2</sub> as heterogeneous semiconductor has received considerable attention for water splitting to produce hydrogen (Fujishima, 1972; Khan, 1999; Mohaputra, 2007) degradation of organic pollutants (Chen, 1999; Burda, 2003; Magalhães, 2004; Demeestere, et al., 2005; Mohamed, 2005; Park, 2005; Xu, 2006; Chiou, 2008), and wastewater treatment (Oppenlander, 2003; Parsons, 2004). However, owing to its wide band gap (3.0–3.2 eV) titanium n- TiO<sub>2</sub> is a UV absorber. Its photoresponse is limited in the ultraviolet part of the solar spectrum, which is only a small fraction (5%) of the sun's energy.

While, the redox potential for conduction band electrons is –0.52 V, which is negative enough to reduce dioxygen to superoxide, or to hydrogen peroxide. Depending upon the exact conditions, the holes, •OH radicals, O<sub>2</sub><sup>•–</sup>, H<sub>2</sub>O<sub>2</sub> and O<sub>2</sub> itself can all play important roles in the photocatalytic reaction mechanisms (Fujishima, 2005).

## 2.5 Mechanism of Photocatalytic Reaction

The heterogeneous photocatalytic reaction is initiated with the absorption of radiation equal to or higher than the band-gap energy ( $E_{bg}$ ) of the target semiconductor.  $E_{bg}$  is defined as the difference between the filled valence band (VB) and the empty conduction band (CB). When photons with energy equal to or higher than  $E_{bg}$  reach the surface of the photocatalyst, they will cause molecular excitation. As a result, mobile electrons will be generated in the higher-energy CB simultaneously with the generation of positive holes in the lower-energy VB of the photocatalyst. After the initiation of photogenerated electron–hole pairs, the photocatalytic reaction will proceed through a series of chemical events. The photogenerated holes and electrons can either recombine and dissipate the

absorbed energy as heat or be available for use in the redox reaction. Photogenerated holes and electrons that do not recombine migrate to the surface of catalyst for redox reaction. The redox reaction will utilize both the electron and hole, with the positive holes ( $h^+$ ) for oxidation processes and the electrons ( $e^-$ ) for reduction processes on the surface of the photocatalysts. The positive holes break apart the water molecule to form hydron (positive hydrogen cation,  $H^+$ ) and the hydroxyl radical ( $OH^\cdot$ ). This  $OH^\cdot$  will then lead to the production of strong oxidizing  $HO^\cdot$  radicals. Meanwhile, the negative electrons react with the oxygen molecule to form a superoxide anion ( $O_2^{\cdot-}$ ). This superoxide anion also produces  $HO^\cdot$  radicals via the formation of  $HO_2^\cdot$  radicals and  $H_2O_2$ . The electron-hole recombination step is undesirable as it will result in process inefficiencies and waste the energy supplied by the photon. Therefore, it is often considered as one of the major factors limiting the efficiency of the photocatalytic processes (Li Puma et al. 2008). The general mechanism of the photocatalytic reaction on light-illuminated  $TiO_2$  is summarized in Table 2.1.

Table 2-1: General mechanism of the photocatalytic reaction on illuminated  $TiO_2$  (Teh & Mohamed 2011).

Process	Reaction steps
Photo-excited $TiO_2$ generates electron-hole pairs ( $h\nu \geq EG$ )	$TiO_2 \xrightarrow{h\nu} e^- + h^+$
Photogenerated holes, $h^+$ migrate to catalyst surface and react with water molecules adsorbed on the catalyst surface	$TiO_2(h^+) + H_2O_{ad} \rightarrow TiO_2 + HO^\cdot + H^+$
$H_2O_{ad}$	
Photogenerated electrons, $e^-$ migrate to catalyst surface and molecular oxygen acts as an acceptor species in the electron-transfer reaction	$TiO_2(e^-) + O_2 \rightarrow TiO_2 + O_2^{\cdot-}$
Reactions of superoxide anions, $O_2^{\cdot-}$	$O_2^{\cdot-} + H^+ \rightarrow HO_2^\cdot$ $O_2^{\cdot-} + 3HO_2^\cdot \rightarrow HO^\cdot + 3O_2 + H_2O + e^-$ $2HO_2^\cdot \rightarrow O_2 + H_2O_2$

photoconversion of hydrogen peroxide to  $\text{H}_2\text{O}_2 + \text{TiO}_2(\text{e}^-) \rightarrow \text{TiO}_2 + \text{HO}^- + \text{HO} \cdot$   
 give more  $\text{HO} \cdot$  free-radical groups

Oxidization of organic adsorbed pollutants ( $\text{S}_{\text{ad}}$ ) by  $\text{HO} \cdot$  onto the surface of the  $\text{TiO}_2$   
 $\text{HO} \cdot + \text{S}_{\text{ad}} \rightarrow \text{Intermediates}$

Overall reaction  $\text{Organic Pollutant} \rightarrow \text{Intermediates} \rightarrow \text{CO}_2 + \text{H}_2\text{O}$

---

## 2.6 Oil palm fiber ash (Biomass Ash)

Biomass ash are fly ash produce from the combustion of biomass product and it does not contain toxic metal which is found in fly ash from coal combustion. The problem faces from the production of fly ash are the disposal and management of large quantities of fly ash generated because the cost for the disposal is high and have big impact to the environment. Therefore, many researchers are doing research to overcome the problem. The research that has been done for the utilization of the fly ash can be seen in Table 2.2. Fly ash is said to be a promising adsorbent for removal of various pollutants because the adsorption capacity of fly ash may be increased after chemical and physical activation (Ahmaruzzaman 2010). Because of its adsorption capability, a new research will be done on Oil palm fiber ash in purifying the seawater. The biomass ash will be used as a support catalyst for the Titanium Dioxide catalyst. This combination will degrade the contamination present in the seawater.

Table 2-2: The research on utilization of fly ash.

Title	Researcher
Use Of Coal Fly Ash As A Catalyst In The Production of Biodiesel	(Ameer 2010)
Synthesis of Nanocrystalline $\text{TiO}_2$ -Coated Coal Fly Ash For Photocatalyst	(Yu 2003)
Favorable Recycling Photocatalyst $\text{TiO}_2/\text{CFA}$ : Effects of Loading Method on The Structural Property And Photocatalytic Activity	(Shi et al. 2009)

---

## 2.7 Metal Loading in Photocatalyst

Titanium dioxide is one of the most efficient photocatalysts for the detoxication of organically charged waste water but this material suffers from the drawback of poor absorption properties because of a band gap of 3.2 eV. The wavelengths of Titanium Dioxide is shorter than 400 nm which are needed for light induced generation of electron±hole pairs. Therefore, many researcher are trying to overcome the band gap problem. One of the way to overcome this problem is doping with transition metal ions for inducing a batho-chromic shift of the band gap. However, this doping changes other physical properties such as lifetime of electron±hole pairs and adsorption characteristics (Wilke & Breuer 1999). The research involving the band gap can be seen in Table 2.3. For this paper, the metal that will be used are Ferum and Nickel. This metal will be mix with Titanium Dioxide and biomass ash with different weight ratio. This mixture will increase the band gap so that the reaction can be done using sunlight and improve the quality of the seawater.

Table 2-3: The research on effect of metal in photocatalyst.

<b>Title</b>	<b>Researcher</b>
Bandgap studies on anatase titanium dioxide nanoparticles	(Reddy et al. 2002)
Role of Fe Doping in Tuning the Band Gap of TiO <sub>2</sub> for the Photo-Oxidation-Induced Cytotoxicity Paradigm	(George et al. 2011)
Preparation and Characterization of Fe <sup>3+</sup> , La <sup>3+</sup> Co-Doped Tio <sub>2</sub> Nanofibers and Its Photocatalytic Activity	(Wu et al. n.d.)
Semiconductor-Metal Composite Nanostructures. To What Extent Do Metal Nanoparticles Improve the Photocatalytic Activity of TiO <sub>2</sub> Films	(Subramanian et al. 2001)

### 3 MATERIALS AND METHODS

#### 3.1 Introduction

For this chapter, there is an explanation of the material used and detailed procedure that were used to run this experiment to achieve the objective of this research. Summarization of the experimental flow chart related to experimental procedure is shown in Figure 3-1.

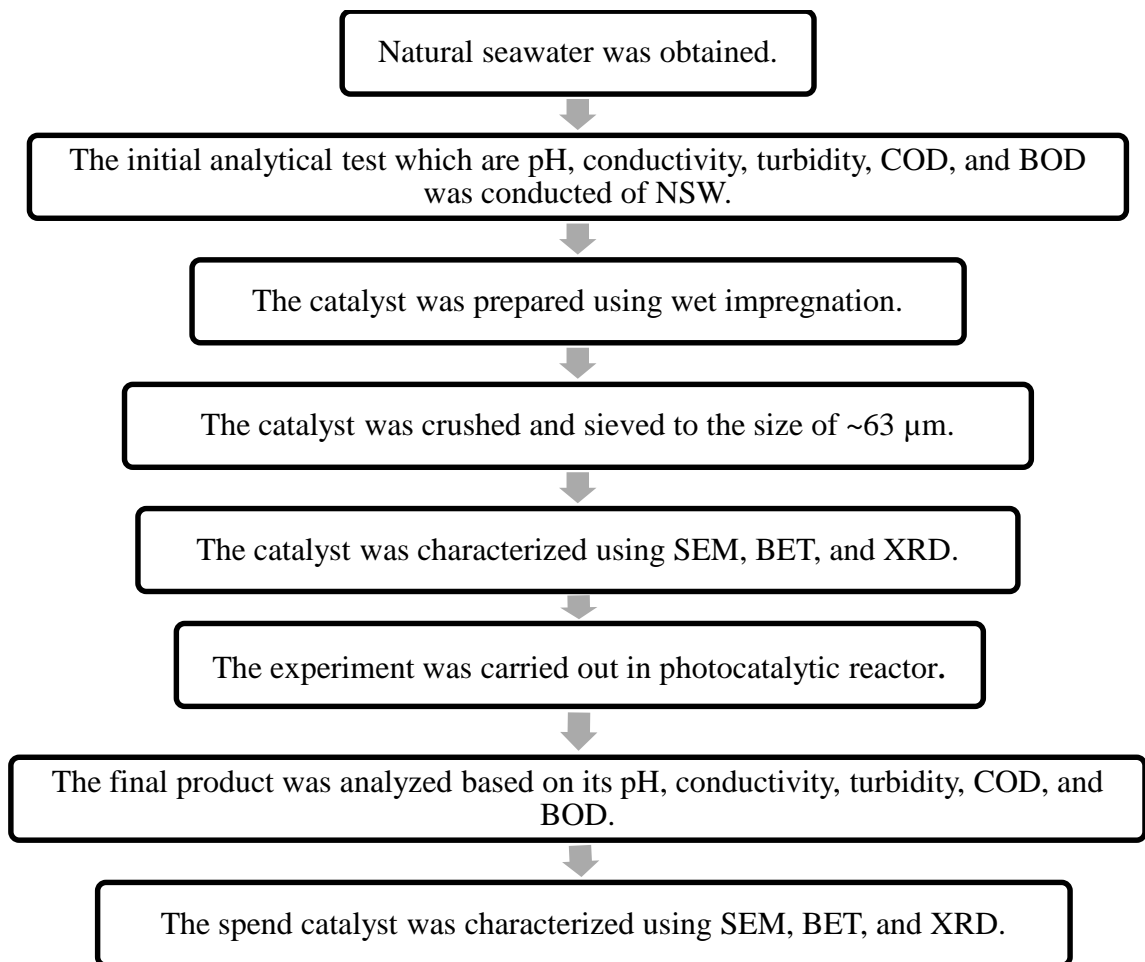


Figure 3-1: Flow diagram of experimental procedure.

## **3.2 Material**

For this research, the raw materials used for photocatalytic reaction preparation were natural seawater (NSW) and palm oil fibre ash (Biomass ash). While the chemicals used for these research were Titanium Dioxide ( $\text{TiO}_2$ ) catalyst, Nickel Nitrate Hexahydrate ( $\text{Ni}(\text{NO}_3)_2 \cdot 6\text{H}_2\text{O}$ ), and Ferum (III) Nitrate nonaydrate ( $\text{Fe}(\text{NO}_3)_3 \cdot 9\text{H}_2\text{O}$ ).

### **3.2.1 Natural Seawater (NSW)**

The NSW sample from Teluk Cempedak Kuantan, Pahang. The sample was stored at 4 °C in the refrigerator.

### **3.2.2 Oil palm fiber ash (Biomass ash)**

Oil palm fiber ash was obtained from Felda Lepar Hilir 3 palm oil mill, Gambang, Kuantan, Pahang. It was used as a catalays supporter for  $\text{TiO}_2$ .

### **3.2.3 Chemical**

The chemical used was  $\text{TiO}_2$  powder with 99% purity, Nickel Nitrate Hexahydrate ( $\text{Ni}(\text{NO}_3)_2 \cdot 6\text{H}_2\text{O}$ ) with 99% purity, Iron(III) Nitrate Nonahydrate ( $\text{Fe}(\text{NO}_3)_3 \cdot 9\text{H}_2\text{O}$ ) with 99% purity. These three chemical was obtained from Sigma-Aldrich Malaysia.

## **3.3 Preparation of Solution and Catalyst**

### **3.3.1 Preparation of NSW**

For the natural seawater, the seawater was obtained from Teluk Cempedak, Kuantan, Pahang. The NSW was stored in a refrigerator at 4 °C. The volume of the NSW used for each experiment was depend on the weight ratio of 1:400 which represent the weight of catalyst and the weight of the NSW respectively.

### 3.3.2 Preparation of Catalyst

For this research, three type of catalyst were produced via wet impregnation. The detail of the catalyst is illustrated in Table 3-1. The solution was stirred by using hot plate at 80°C for four hours. The solution was then dried overnight at 100°C in the oven. After that, the solution was calcined at 500°C for four hours in the furnace. The solution was then crushed and sieved to the size of ~63µm.

Table 3-1: The weight ratio of the three catalyst.

Catalyst	Weight Ratio (%)		
	TiO <sub>2</sub>	Biomass Ash	Metal(Nickel/Ferum)
No metal loading	50	50	0
Nickel loading	45	45	10
Ferum loading	45	45	10

### 3.3.3 Characterization of Catalyst

The fresh and used catalyst were characterized by using X-ray Diffraction (XRD), Scanning Electron Microscopy (SEM) and Brunauer Emmett Teller (BET). The catalyst was characterized by using XRD to determine the crystal structure of the catalyst. While SEM was used to determine the catalyst's surface mophology. BET surface analysis was used to measure the total specific surface area, pore size and pore volume of the catalyst.

#### 3.3.3.1 Scanning Electron Microscopy (SEM)

SEM (CAEL ZEISS) was used for catalyst characterization and surface morphology analysis. A high resolution SEM coupled to an energy dispersive X-tray spectrometer system was producing various signals contained the information regarding the sample's surface topography and composition. Then the samples were mounted on a stub of metal with adhesive, coated with 40 - 60 nm of metal such as Gold/Palladium and then were observed in the microscope.



Figure 3-2: Scanning Electron Microscopy (SEM).

### 3.3.3.2 Brunauer Emmett Teller (BET)

BET (Micromeritics ASAP2020) surface analysis was used for measuring the total specific area, pore size, and pore volume of the catalysts. This instrument provide precise evaluation of material by nitrogen multilayer adsorption measured as a function of relative pressure using fully automated analyzer. The samples were degassed in a vacuum at high temperatures. The highest temperature possible that will not damage the sample's structure is usually chosen in order to shorten the degassing time. IUPAC recommends that samples be degassed for at least 16 hours to ensure that unwanted vapors and gases are removed from the surface of the sample. About of 0.5 g of sample was required for the BET to successfully determine the surface area. Then the samples were placed in glass cells to be degassed at 200 °C for six hours and then analyzed by the BET machine.



Figure 3-3: Brunauer Emmett Teller (BET).

### 3.3.3.3 X-ray Diffraction (XRD)

XRD (ADX-2500) was used to determine the composition of the catalyst. The XRD technique takes a sample of the material and places a powdered sample on a holder, then the sample was illuminated with x-rays of a fixed wave length and the intensity of the reflected radiation was recorded using goniometer. The data then analysed for the reflection angle to calculate the inter atomic spacing.



Figure 3-4: X-Ray Diffraction (XRD).

### 3.4 Photocatalytic Reactor Set Up

The photocatalytic reactor (Figure 3-5) with a diameter of eight centimeters and height of 30 cm was set up consisting of black box, cooling fan, temperature controller, reactor, hot plate, magnetic stirrer, silicon tubing and mercury light. The mercury light was placed beside the reactor at distance at three centimeter. The experiment was run inside the black box to prevent the UV light exposure to the surrounding environment.

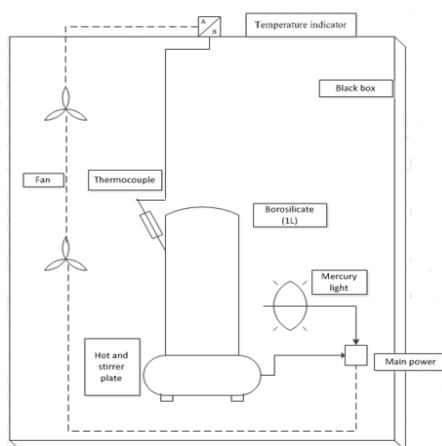


Figure 3-5: The schematic diagram of photocatalytic reactor

### **3.5 Experimental Procedure**

The seawater sample and catalyst was tested its effectiveness in the production of clean water sample by using the one liter borosilicate glass in photocatalytic reactor. The catalyst to seawater sample performed was used according to the weight ratio of 1:400. The magnetic stirrer was put in the mixture to make sure the solution was well mixed. The reactor with mercury light of 365 nm or 420 nm wavelength emission was used in the investigation. The experiments were carried out for two hours and the mixing speed was 6000 rpm.

### **3.6 Analytical Test**

The seawater was analyzed based on the pH, Conductivity, Chemical Oxygen Demand (COD), Total Dissolve Solid (TDS), Chemical Oxygen Demand (COD), Biochemical Oxygen Demand (BOD) and Turbidity. The seawater sample analysis was determined before and after the experiment

#### **3.6.1 pH, Conductivity and Total Dissolved Solid (TDS)**

For the value of pH, conductivity and total dissolved solid (TDS), it were measured using Hach MM150 pH, conductivity and TDS meter. pH was a measure of liquid acidity and alkalinity based on the quantity of hydrogen ion ( $H^+$ ) the solution contain. While conductivity was a measure of the ability of water to pass an electrical current. Conductivity in water was affected by the presence of inorganic dissolved solids such as chloride, nitrate, sulfate, and phosphate anions (ions that carry a negative charge) or sodium, magnesium, calcium, iron, and aluminum cations (ions that carry a positive charge). TDS were the total amount of mobile charged ions, including minerals, salts or metals dissolved in a given volume of water, expressed in units of mg per unit volume of water (mg/L), also referred to as parts per million (ppm). The three value were obtained by immersing the probe in the solution. The value was measured before and after the experiment to observed changes in value.



Figure 3-6: pH, conductivity and TDS meter.

### 3.6.2 Chemical Oxygen Demand (COD)

Chemical oxygen demand (COD) was used as a measure of oxygen requirement of a sample that is susceptible to oxidation by strong chemical oxidant. The mg/L COD results were defined as the mg of O<sub>2</sub> consumed per liter of sample under conditions of this procedure. For the COD procedure, the sample was heated at 150 °C for two hours with a strong oxidizing agent, potassium dichromate using the COD digestion reactor (HACH DRB 200). After two hours, the sample was let cool until it reach the room temperature. Then the sample was transferred to the COD spectrophotometer (HACH DR2800) to obtain the COD value. The COD of the initial solution and the final product was measured.

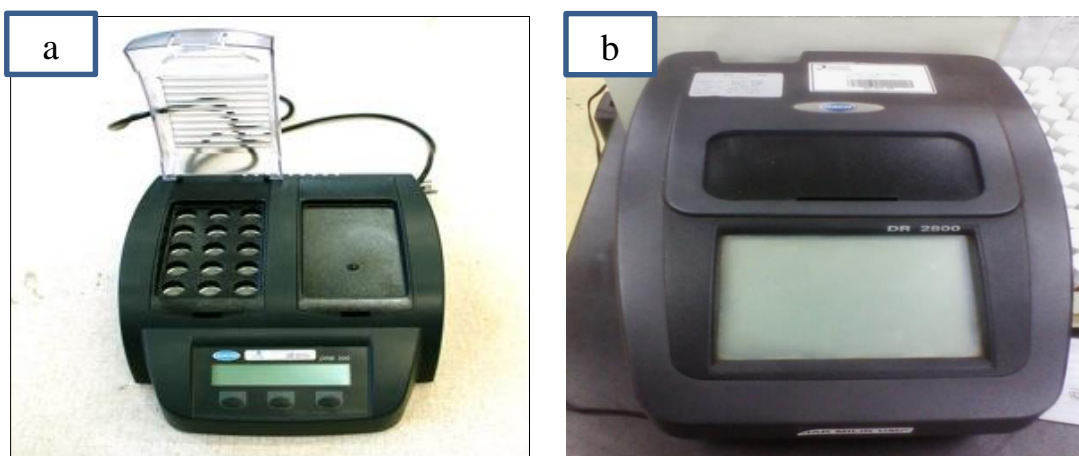


Figure 3-7: COD measuring equipment (a) COD digestion reactor (b) COD spectrophotometer

### 3.6.3 Biochemical Oxygen Demand (BOD)

Biochemical oxygen demand (BOD) test measures the ability of naturally occurring microorganisms to digest organic matter, usually in 5 days incubation at 20°C by analyzing the depletion of oxygen. BOD can also be used to evaluate the efficiency of treatment processes, and is an indirect measure of biodegradable organic compounds in water. The BOD test is normally required by a regulatory program. For this experiment, BOD<sub>5</sub> will be examined by dilution method (Standard Method 5210B). The reagent which were Phosphate buffer solution, Magnesium Sulfate solution, Calcium Chloride solution and Ferric Chloride solution was prepared first which was used to prepare dilution water. 300 ml of dilution water was mixed with 10 ml of the NSW sample in an incubator bottle. The solution pH was adjusted between 6.5-7.5 by adding alkali or acid. Then the dissolve oxygen meter was used to measure the dissolved oxygen. Then the sample solution was put in an incubator chamber for 5 days at 20 °C. After five days, the dissolved oxygen value was measured. Then the two dissolved oxygen value was used to calculate the BOD value using these formula  $BOD_5, \text{ mg/L} = (D_1 - D_2) / P$ . D<sub>1</sub> represent the initial dissolve oxygen while D<sub>2</sub> represent the final dissolved oxygen. P represent Decimal volumetric fraction of sample used. The BOD of the initial solution and final product was measured using dissolved oxygen meter (YSI 5100).



Figure 3-8: Dissolved oxygen meter.

## 4 RESULT AND DISCUSSION

### 4.1 Introduction

This chapter described the effect of metal loading and wavelength in photocatalytic reaction in seawater desalination where different catalyst was used. The catalyst used in these research were no metal loading catalyst, nickel loading catalyst and ferum loading catalyst. These chapter also showed the analysis of the seawater on the Ph, conductivity, TDS, COD, and BOD before and after the experiment. There were also the characterization of the fresh and spend catalyst by using SEM, BET, and XRD.

### 4.2 Property of Seawater Sample

For these investigation, seawater was used. The seawater sample was obtained at Teluk Cempedak, Kuantan, Pahang. The seawater sample pH, conductivity or also known as salt concentration, total dissolved solid (TDS), BOD and COD was analyzed. The fresh seawater was analyzed several times and the average reading can be seen in Table 4-1.

Table 4-1: Fresh NSW analysis

Sample	Conductivity		TDS	BOD	COD
	Ph	(mS/cm)	(g/L)	(mg/L)	(mg/L)
<b>Fresh seawater</b>	8.2	48.8	31.3	33.03	669

From table 4- 1, it is found that the pH value was at 8.2 which was in the alkaline range, while the conductivity was 48.8 mS/cm, the TDS was at 31.3 g/L. In addition, the BOD was at 33.03 mg/L and COD was at 669 mg/L.

### 4.3 The Effect of Metal Loading

These experiment focus on the study of the effect of metal loading whether there were improvement by the addition of the metal loading to the hybrid TiO<sub>2</sub> and biomass ash catalyst. For these investigation, there were two type of metal loading used, nickel and ferum. These metal loading was added to the hybrid catalyst during the preparation of catalyst which was via wet impregnation. The image of the catalyst produce under the SEM shown in Figure 4-1(a) was the hybrid catalyst with no metal loading, Figure 4-1(b) hybrid catalyst with nickel loading and Figure 4-1(c) was the hybrid catalyst with ferum loading. The function of the SEM was to investigate the morphology of the catalyst. From the SEM images, it was found that the TiO<sub>2</sub> crystalline and the metal loading was well dispersed around the biomass ash. According to Jamo et. al (2013), the biomass ash has flat and smooth structure, irregular particle and porous structure. While for the TiO<sub>2</sub> and metal loading has crystalline structure that was why the TiO<sub>2</sub> and the metal loading was well dispersed around the biomass ash.

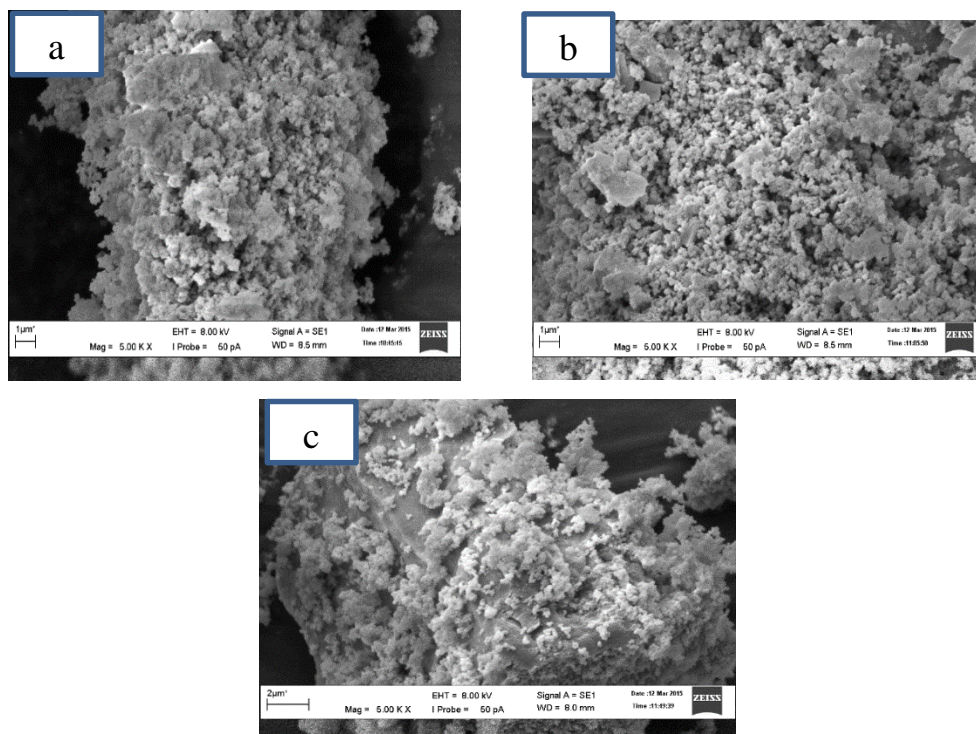


Figure 4-1: SEM image of the fresh catalyst: a) no metal b) with nickel loading c) with ferum loading

After the preparation of the catalyst, the catalysts were tested through the photocatalytic reaction. The light used for the photocatalytic reaction was at 365 nm wavelength. The reaction was conducted for two hours. After the reaction was done, the seawater was analyzed for its pH, conductivity, TDS, BOD and COD. The result of the water analysis after the reaction is tabulated in table 4-2.

Table 4-2: NSW analysis after the photocatalytic reaction.

Sample	Ph	Conductivity (mS/cm)	TDS (g/L)	BOD (mg/L)	COD (mg/L)
<b>Fresh NSW</b>	8.20	48.8	31.3	33.03	669
<b>No metal loading</b>	8.04	47.8	30.6	15.27	100
<b>Nickel loading</b>	8.14	46.9	30.5	10.50	80
<b>Ferum loading</b>	8.40	47.7	30.6	19.26	101

From Table 4-2, it is found that there was an improvement of the water quality compared to the fresh seawater especially for the conductivity, TDS, BOD and COD. For the pH, there are only reduction for the no metal loading catalyst and nickel loading catalyst while there is increment for ferum loading catalyst. The percentage of the overall reduction is illustrated in Figure 4-2.

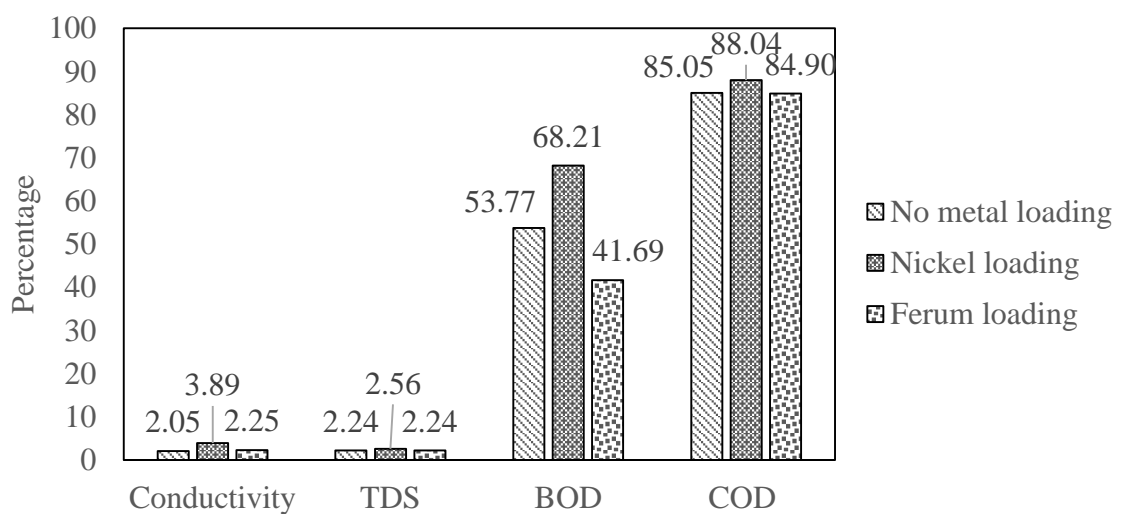


Figure 4-2: Percentage of reduction for the NSW analysis.

For the no metal loading catalyst, the conductivity was reduce from 48.8 mS/cm to 47.8 mS/cm which the reduction was at 2.05%, when adding metal loading, the conductivity reduction improved where the conductivity value of the seawater was reduced at 3.89% which reduce from 48.8 mS/cm to 46.9 mS/cm for the nickel loading catalyst. For the ferum loading the reduction was at 2.25% which was from 48.8 mS/cm to 47.7 mS/cm and it is smaller than nickel. The reduction of conductivity is shown in Figure 4-3 and it is found that the nickel loading catalyst has the highest reduction for conductivity. The conductivity of the seawater represent the value of the salt concentration. Higher the conductivity the higher the salinity of the seawater. Usually, the water that was high in conductivity will become a good conductor due to the presence of positive ion and negative ion that can donate and accept electrons.

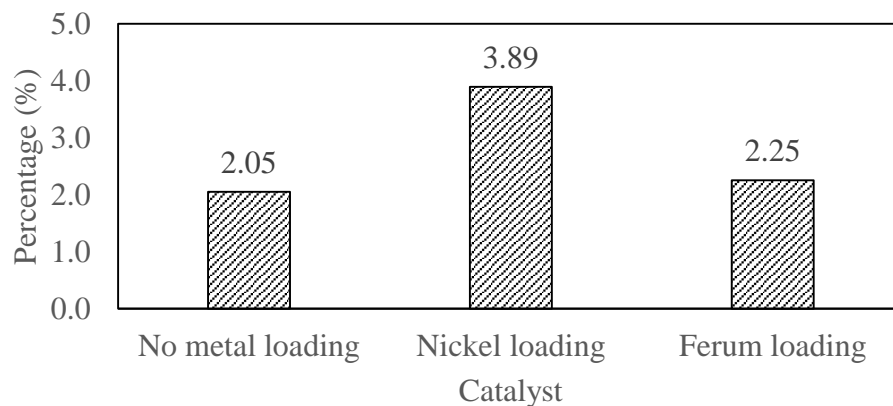


Figure 4-3: Percentage of reduction for the conductivity of NSW analysis.

For the TDS, the reduction for the no metal loading catalyst was 2.24% which reduced from 31.3 g/L to 30.6 g/L. For the nickel loading, the TDS reduced from 31.3 g/L to 30.5 g/L. The percentage of reduction is 2.56%. While the ferum loading catalyst, the TDS decreasing form 31.3 g/L to 30.6 g/L. The Percentage of reduction for the ferum loading is similar with the no metal loading catalyst which is 2.24%. The TDS reduction for the three catalyst can be seen in Figure 4-4. From the figure, it is found that nickel has the highest reduction compared to no metal loading and ferum loading catalyst.

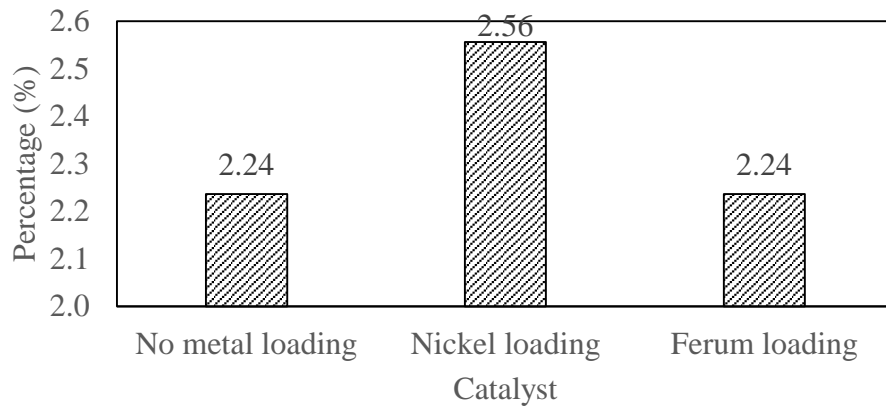


Figure 4-4: Percentage of reduction for the TDS of NSW analysis.

From conductivity and TDS data, it was found that the catalyst has the ability to absorb the salt content in the seawater and these was supported with the data obtained from the used catalyst analysis using XRD analysis which function to determine the crystalline structure at the catalyst. Beside salt, the XRD analysis also found the crystalline of the  $\text{TiO}_2$ , biomass ash and metal. According to Figure 4-5, the XRD patterns showed that the  $\text{TiO}_2$  have a predominant crystal structure of anatase type and fiber ash exhibited the characteristic peaks of crystalline phase of quartz. It is show that the crystal structure of anatase obtained in the catalyst have a high photoactivity in purifying the seawater and the anatase phase is more photoactive than rutile (Ahmed et.al,2011). The decrease in TDS value also showed that the catalyst was not soluble in the seawater and according to Davis et. al (2010),  $\text{TiO}_2$  was not insoluble in water (Davis et.al, 2010). The biomass ash also which contained silica does not soluble in water and could be easily separated from water. Therefore the TDS of the seawater was not affected by the catalyst.

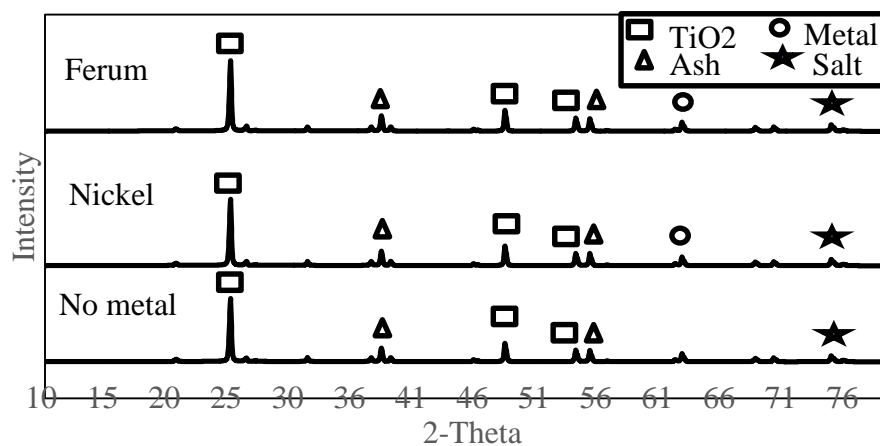


Figure 4-5: XRD analysis for the metal loading catalyst.

Table 4-3: BET analysis for the metal loading catalyst.

Type of Catalyst	Specific surface area (m <sup>2</sup> /g)		Pore volume x10 <sup>2</sup> (cm <sup>3</sup> /g)		Pore size (nm)	
	Before treatment	After treatment	Before treatment	After treatment	Before treatment	After treatment
<b>No metal loading</b>	22.75	13.83	0.47	0.39	1.28	1.16
<b>Nickel loading</b>	13.25	16.75	0.34	0.45	1.19	1.11
<b>Ferum loading</b>	12.36	13.71	0.28	0.34	1.18	1.11

These also supported by the data obtain from the BET analysis where the data obtained were the specific surface area, pore volume and pore size. The data can be seen in Table 4-3, where there was an increment of the specific surface area, and pore volume and the reduction of pore size after the photocatalytic reaction. The no metal loading catalyst specific surface area was 22.75 m<sup>2</sup>/g and reduced to 13.83 m<sup>2</sup>/g. For the specific surface area of the nickel loading catalyst, the area increase from 13.52 m<sup>2</sup>/g to 16.75 m<sup>2</sup>/g which was around 23.89% increment. While for the ferum loading the specific surface area increases from 12.36 m<sup>2</sup>/g to 13.71 m<sup>2</sup>/g which was around 10.92% increment.

For the pore volume, the no metal loading catalyst had a reduction in pore volume which was from 0.47 cm<sup>3</sup>/g to 0.39 cm<sup>3</sup>/g. The nickel loading catalyst had an increment from 0.34 cm<sup>3</sup>/g to 0.45 cm<sup>3</sup>/g which was at 32.35% increment and the ferum loading catalyst had an increment around 21.43% increment which was from 0.28 cm<sup>3</sup>/g to 0.34 cm<sup>3</sup>/g.

For the pore size, there was a reduction for the three catalyst which was because the salt might be attach to the pore of the catalyst. The pore size of the no metal loading catalyst decreases from 1.28 nm to 1.16 nm which was around 9.38%. For the nickel loading catalyst decreases from 1.19 nm to 1.11 nm where the reduction was at 6.72 %. While for the ferum loading catalyst, the pore size reduced up to 5.93% which was from 1.18 nm to 1.11 nm.

From the BET analysis, it showed that there were increment in specific surface area and pore volume for the metal loading catalyst while for the no metal there was a reduction. Even though there was reduction, it was still proven that the no metal loading catalyst able to absorb salt where the pore size reduced after the experiment. The reduction in the specific area and pore volume of no metal loading catalyst might due to the breakage of the catalyst structure after the experiment. These also show that, the addition of metal loading to the hybrid catalyst not only improve the catalyst performance but also strengthen it structure. Table 4-3 also show that, the nickel loading has higher increment of specific surface area and pore volume compared to the ferum loading and the no metal loading catalyst. These shows that nickel loading catalyst absorb more salt than ferum and no metal loading catalyst.

From Figure 4-6, it is also found that, there was reduction for BOD where the reduction for the no metal loading was at 53.77% which was from 30.03 mg/l to 15.25 mg/l. For the nickel loading catalyst, the reduction was at 68.21% which was from 30.03 mg/l to 10.5 mg/l. For the ferum loading, the value decrease from 30.03 mg/l to 19.6 mg/l which was around 41.69%. Figure 4-7 also showed that nickel loading catalyst has the highest BOD reduction compared to the no metal loading and ferum loading catalyst. The BOD test occurred in 5 days due to using BOD<sub>5</sub> analysis. The BOD value was calculated based on the value of dissolved oxygen obtained from before and after the five days. It was measured using Dissolved oxygen meter. During the five days, the sample was incubated under 20 °C. The BOD showed the value of the oxygen consumed by the microorganism in the seawater. If the value was high, the number of microorganism in the water also high. From the data also, it was found that nickel loading show the highest reduction of BOD followed by the no metal loading and ferum loading.

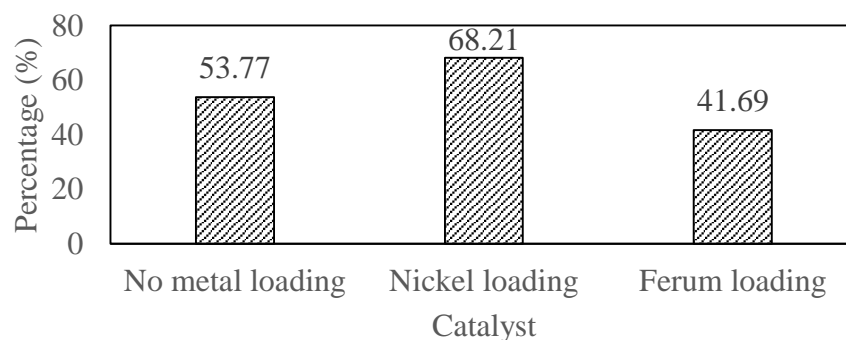


Figure 4-6: Percentage of reduction for the BOD of NSW analysis.

Figure 4-7 shows that the no metal loading catalyst able to reduce the COD up to 85.05% which was from 669 mg/l to 100 mg/l. The nickel loading catalyst able to reduce up to 88.04% which was from 669 mg/l to 80 mg/l. For the ferum loading catalyst, the COD reduced from 669 mg/l to 101 mg/l which was around 84.9%. From these data, it showed that nickel loading had the highest reduction followed by no metal loading catalyst and ferum loading catalyst. COD was used to measure the mineralization effects of samples degradation of the water. It is shown that some of catalyst has the potential to decrease the COD values. Based on the Shinde et. al., (2011) investigation, the mineralization needs a longer reaction time to lower the COD values. And, their studies also reveals that the degradation effect of seawater to CO<sub>2</sub> by measuring COD value show the decreasing of COD values with circulation of time.

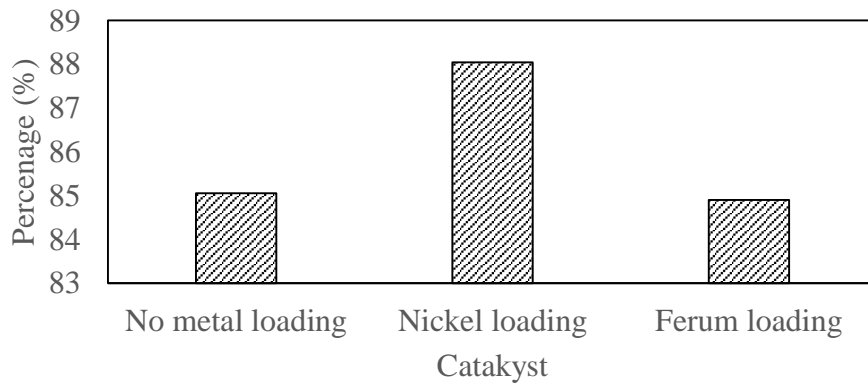


Figure 4-7: Percentage of reduction for the COD of NSW analysis.

Figure 4-4 showed the SEM image of the no metal loading catalyst, nickel loading catalyst and ferum loading catalyst before and after the experiment where can be seen the structure is not ruptured and there is crystalline structure increase at the surface of the catalyst which might be salt that attach at the surface of the catalyst after the experiment. Because the structure of the catalyst do not rupture, further analysis should be done to investigate the durability of the catalyst.

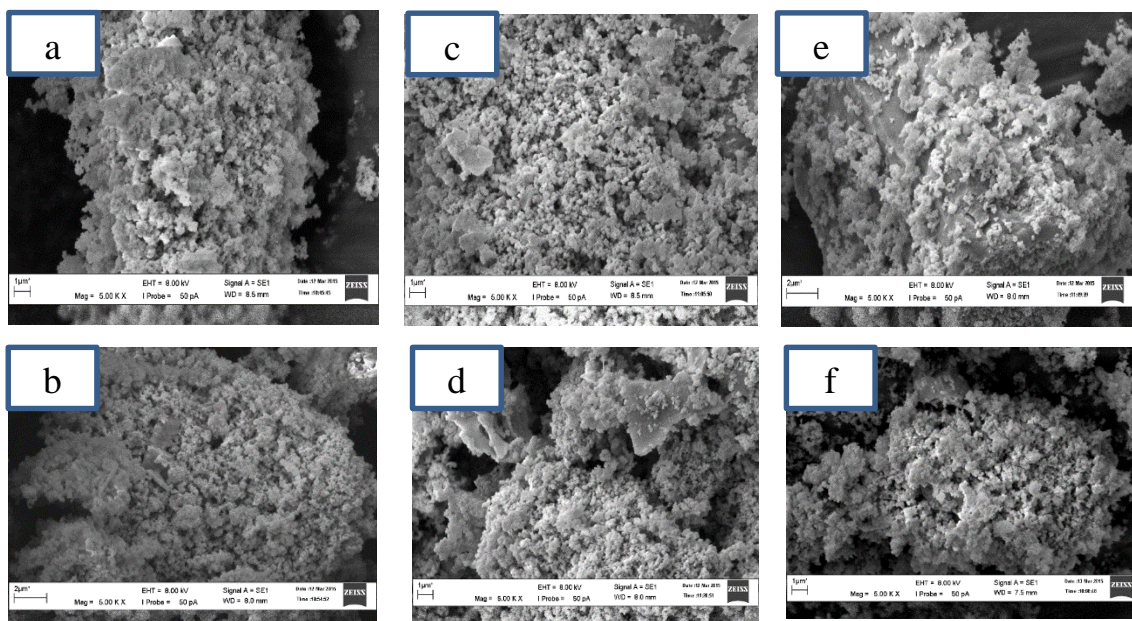


Figure 4-8: SEM image of the used catalyst: (a) fresh no metal loading (b) used no metal loading (c) fresh nickel loading (d) used nickel loading (e) fresh ferum loading (f) used ferum loading

From the overall data, it was found that nickel loading catalyst had the best overall performance compared to the two catalyst which were no metal loading catalyst and ferum catalyst. These was because nickel loading catalyst had the highest reduction in conductivity, TDS, BOD and COD which can be seen at Figure 4-2. These also show that the addition of nickel to the hybrid catalyst help to improve the performance of the catalyst.

#### 4.4 The Effect of Wavelength

For the investigation also, the metal loading catalyst also tested using different wavelength light. It was done in order to study whether the different light wavelength affect the performance of the catalyst. The steps for these investigation was similar with the previous investigation which the experiment was conducted for two hours using the photocatalytic reactor. The mixing speed was set at 6000 rpm. The difference only in the wavelength where the previous investigation the light used had 365 nm wavelength while for these investigation 420 nm wavelength was used. The type of metal loading catalyst also similar from the previous which were no metal loading catalyst, nickel loading

catalyst and ferum loading catalyst where the SEM images can be seen at Figure 4-1. Table 4-4 show the overall data obtained from the NSW analysis.

Table 4-4: NSW analysis after the photocatalytic reaction at 420 nm.

<b>Sample</b>	<b>Ph</b>	<b>Conductivity (mS/cm)</b>	<b>TDS (g/L)</b>	<b>BOD (mg/L)</b>	<b>COD (mg/L)</b>
<b>Fresh NSW</b>	8.2	48.8	31.3	33.03	669
<b>No metal loading</b>	8.02	51.1	32.7	15.75	168
<b>Nickel loading</b>	8.16	49.9	31.9	1.5	53
<b>Ferum loading</b>	8.03	50.1	32	0.9	36

#### 4.4.1 No Metal Loading

No metal loading catalyst is a catalyst that contain TiO<sub>2</sub> and biomass ash with the weight ratio of 50:50. These catalyst was tested using the same reactor as the study of metal loading but with different wavelength which was 420 nm. The experiment was run for two hours. Table 4-5 shows the comparison for the NSW analysis for no metal loading catalyst at 365 nm wavelength and 420 nm wavelength.

Table 4-5: NSW analysis for no metal loading catalyst.

<b>Sample</b>	<b>Ph</b>	<b>Conductivity (mS/cm)</b>	<b>TDS (g/L)</b>	<b>BOD (mg/L)</b>	<b>COD (mg/L)</b>
<b>Fresh NSW</b>	8.20	48.8	31.3	33.03	669
<b>365 nm</b>	8.04	47.8	30.6	15.27	100
<b>420 nm</b>	8.02	51.1	32.7	15.75	168

Table 4-5 shows that there is a reduction of Ph, conductivity, TDS, BOD and COD for the analysis using the 365 nm wavelength light. While for the 420 nm wavelength light, there are only reduction for the pH, BOD and COD. For the conductivity and TDS, there are increment in value.

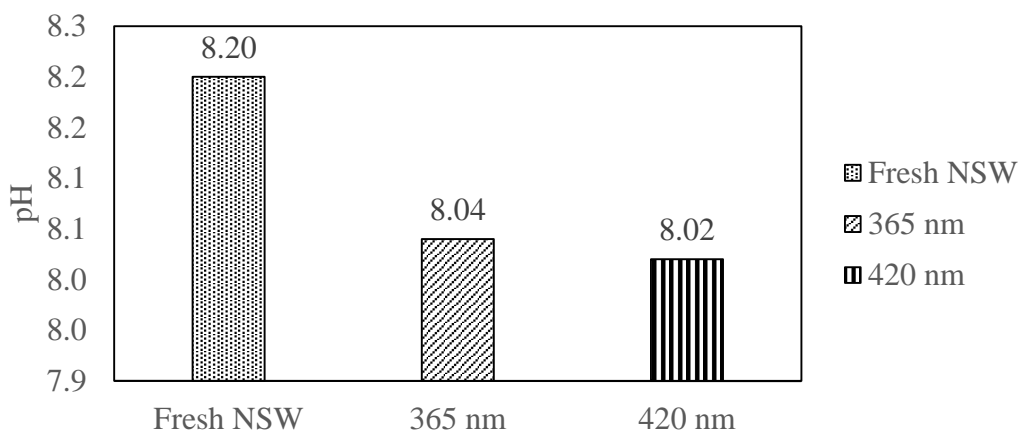


Figure 4-9: NSW analysis for pH.

Figure 4-9 shows the value for the pH for the fresh NSW and the NSW after testing with 365 nm and 420 nm wavelength. While Figure 4-10 show the percentage of reduction for the pH value for the both wavelength light. The initial value for the NSW before the experiment was 8.20. The value then reduce to 8.04 when using the 365 nm wavelength light. These reduction is at 1.95%. While the value of Ph reduce to 8.02 when using the 420 nm wavelength light. The percentage of reduction is at 2.2%.

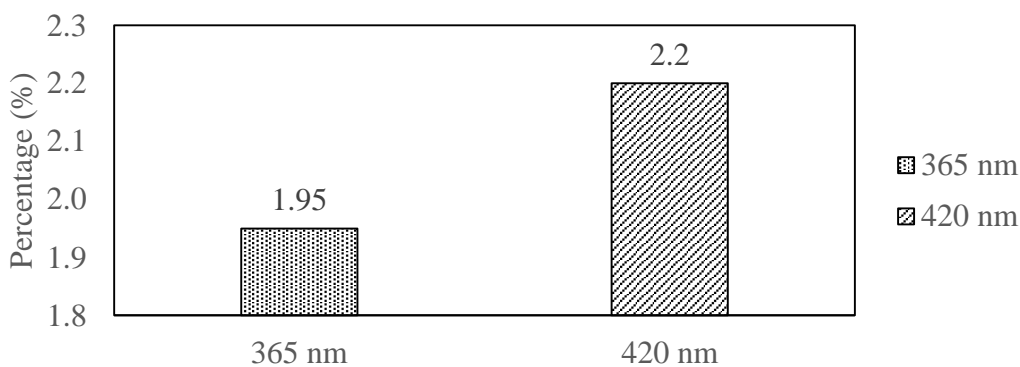


Figure 4-10: Percentage of reduction for pH.

From these data, it is found that the 420 nm wavelength light has the higher reduction of pH compared to the 365 nm wavelength light for the metal loading catalyst. The percentage of reduction difference between these two are at 0.25%.

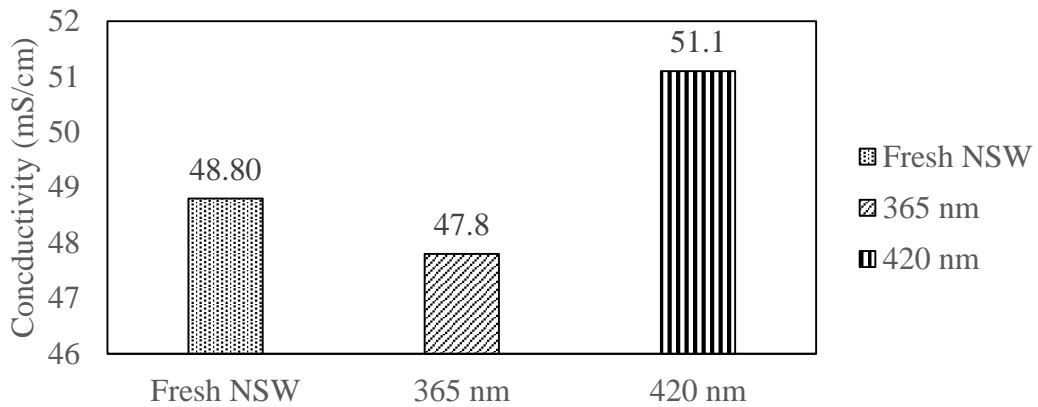


Figure 4-11: NSW analysis for conductivity.

Figure 4-11 shows the value for the conductivity for the fresh NSW and the NSW after testing with 365 nm and 420 nm wavelength. For the conductivity, there is only reduction for the 365 nm wavelength light. While for the 420 nm wavelength light has an increment of value. The 365 nm wavelength light has a reduction of conductivity from 48.8 mS/cm to 47.8 mS/cm. The percentage of reduction is at 2.05%. For the 420 nm wavelength light, the value for conductivity increase from 48.8 mS/cm to 51.1 mS/cm. The increment percentage was at 4.5%. These increment was due to the domination of distillation process where 50 ml of distillate was produced.

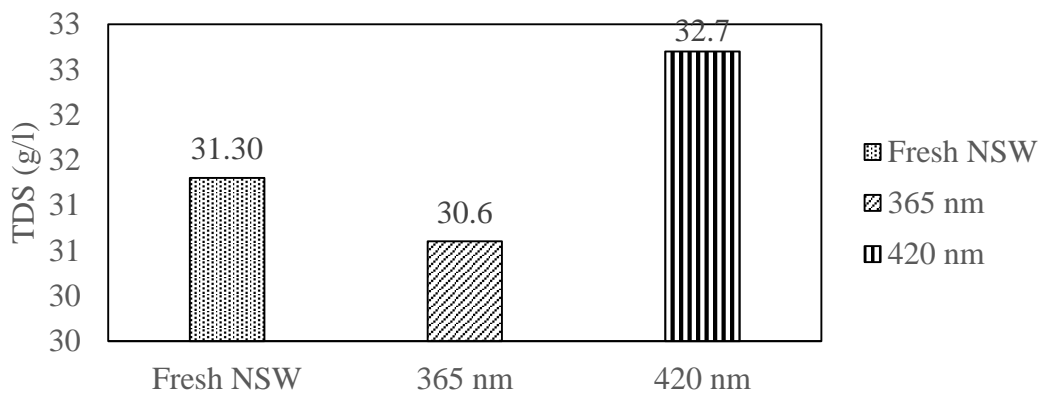


Figure 4-12: NSW analysis for TDS.

Figure 4-12 shows the value for the TDS for the fresh NSW and the NSW after testing with 365 nm and 420 nm wavelength. For the conductivity, there is only reduction for the 365 nm wavelength light. While for the 420 nm wavelength light has an increment of value. The initial value for the TDS is 31.3 g/l. These NSW TDS value decrease to

30.6 g/l for the 365 nm wavelength light. The percentage of reduction is at 2.24%. For the 420 nm wavelength light has an increment to 32.7 g/l. The percentage for the increment is at 4.47%.

From the data obtained for the conductivity and TDS, it can be concluded that the catalyst work best at 365 nm wavelength light where there is reduction for the conductivity and TDS.

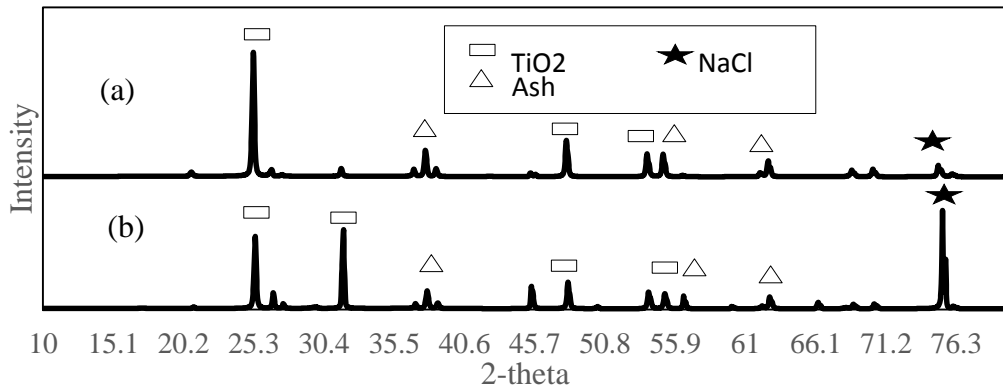


Figure 4-13: XRD analysis (a) 365 nm (b) 420 nm.

The reduction of conductivity and the TDS for the 365 nm wavelength can be proven based the XRD analysis which is illustrated in Figure 4-13. It is found that there is the presence of salt in the XRD analysis. These show that the catalyst has the ability to absorb salt. For the 420 nm wavelength light, even though there is no reduction of conductivity and TDS, there is still absorption of salt. These is proven with the XRD analysis for the 420 nm wavelength light. These is due to the presence of salt in the XRD analysis shown in Figure 4-13.

Table 4-6: BET analysis for no metal loading catalyst

Type of Wavelength	Specific surface area (m <sup>2</sup> /g)		Pore volume x10 <sup>2</sup> (cm <sup>3</sup> /g)		Pore size (nm)	
	Before treatment	After treatment	Before treatment	After treatment	Before treatment	After treatment
365 nm	22.75	13.83	0.47	0.39	1.28	1.16
420 nm	22.75	13.83	0.47	0.43	1.28	1.16

Beside XRD analysis, the reduction of conductivity and TDS can also prove using BET analysis illustrated in Table 4-6. The BET analysis covers three parameter which are the specific surface area, pore volume, and pore size. For the 365 nm and 420 nm wavelength light, the decrease value for the specific surface area are the same which reduce from 22.75 m<sup>2</sup>/g to 13.83 m<sup>2</sup>/g. Which is at 39.2% decrease in area.

For the pore volume, the 365 nm wavelength has a decrease from 0.0047 cm<sup>3</sup>/g to 0.0039 cm<sup>3</sup>/g which is at 17% decrease. While for the 420 nm wavelength, the pore volume decrease from 0.0047 cm<sup>3</sup>/g to 0.0043 cm<sup>3</sup>/g which is at 8.5% decrease in size. Supposedly, the two parameter which are the specific area and the pore volume should have increase in area and volume due to the salt absorption. These decrease of area and volume might be due to the structure break down after the experiment.

For the pore size, the 365 nm and 420 nm has a reduction which is from 1.28 nm to 1.16 nm. From these it is proven that the catalyst absorb salt due to the decrease of pore size.

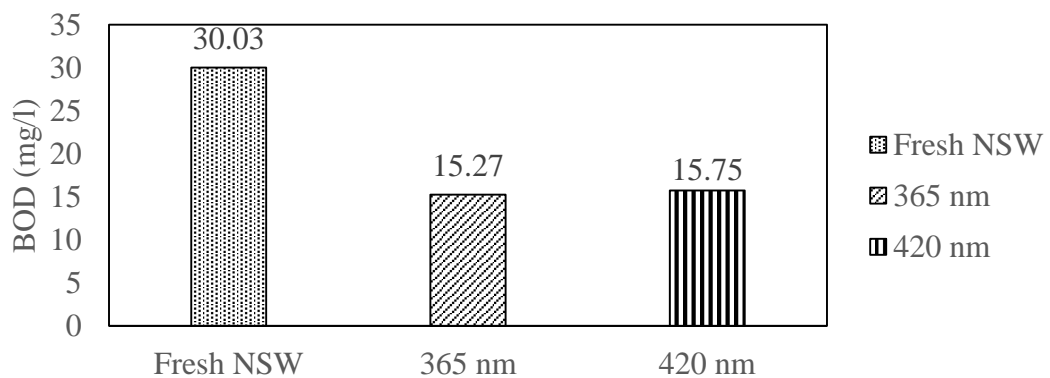


Figure 4-14: NSW analysis for BOD.

Figure 4-14 shows the value of BOD for the 365 nm and 420 nm wavelength light while Figure 4-15 show the percentage of reduction of BOD of the two wavelength. The initial value for the NSW BOD is 30.03 mg/l. These value is reduced to 15.27 mg/l when using the 365 nm wavelength light. The percentage of reduction is at 53.7%. While for the 420 nm wavelength light, the initial value reduce to 15.75 mg/l which is at 52.33% of reduction.

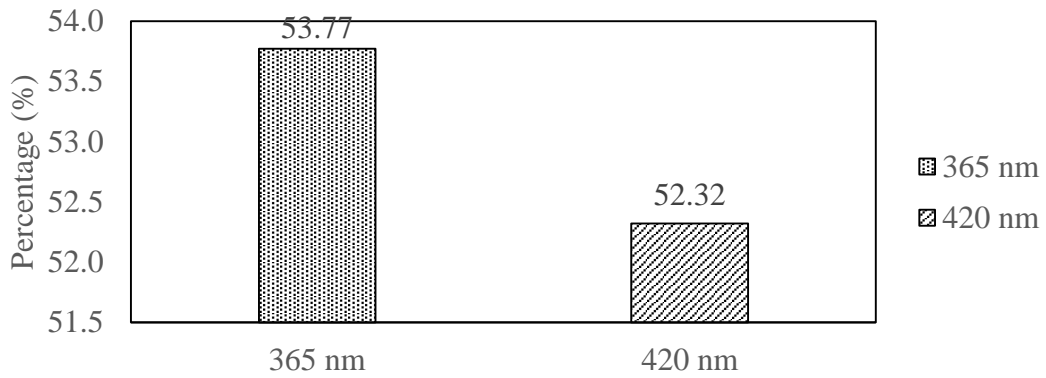


Figure 4-15: Percentage of reduction for BOD.

From these data, it is found that the 365 nm wavelength has the higher BOD reduction compared to the 420 nm wavelength light. The difference of reduction between the two wavelengths is 1.45% which is quiet small.

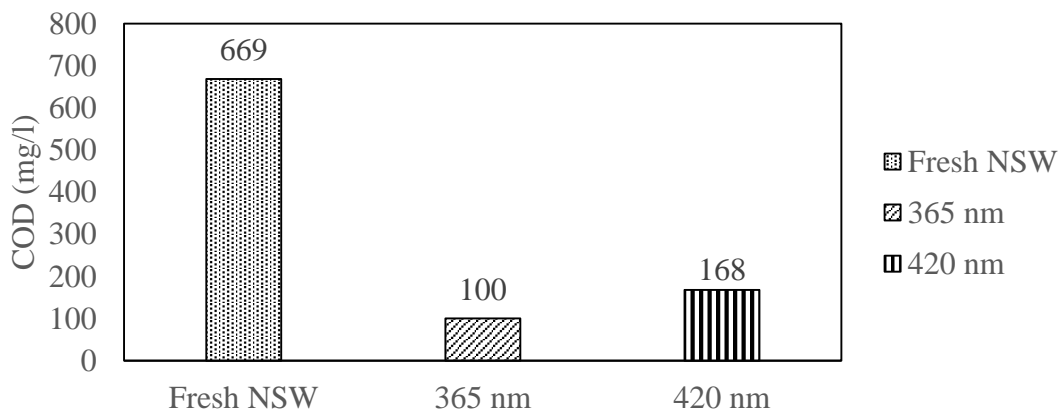


Figure 4-16: NSW analysis for COD.

Figure 4-16 shows the value of COD for the 365 nm and 420 nm wavelength light while Figure 4-17 show the percentage of reduction of COD of the two wavelength. The initial value for the NSW COD is 669 mg/l. The 365 nm wavelength has reduce the initial value of NSW to 100 mg/l which at 85.05% of reduction. While 420 nm wavelength has the ability to reduce the initial value of NSW to 168 mg/l. The percentage of reduction is at 74.89%.

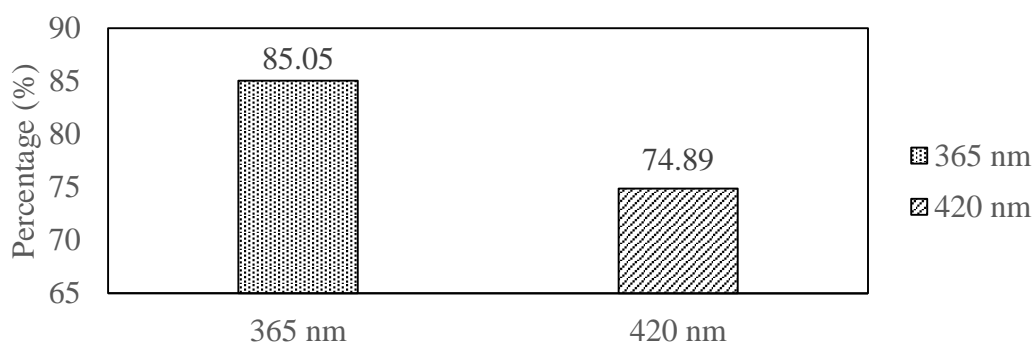


Figure 4-17: Percentage of reduction for COD.

From these two figure, it is found that the no metal loading has higher reduction of COD at 365 nm wavelength light compared to 420 nm wavelength light. These is due to the drop of performance of the reduction of COD.

From all the data obtained for no metal loading catalyst, it is found that the no metal loading catalyst has a drop of performance at 420 nm wavelength light compared to the 365 nm wavelength light. These was due to the percentage of reduction for the conductivity, TDS, BOD, and COD drop in value when tested at 420 nm wavelength. These also show that the band gap of TiO<sub>2</sub> which is between 3.0-3.2 eV (Fujishima, 2005), is not suitable to be used at wavelength 420 nm.

#### 4.4.2 Nickel Loading

Nickel loading catalyst is a catalyst that contain TiO<sub>2</sub>, biomass ash, and nickel with the weight ratio of 45:45:10. These catalyst was tested using the same reactor as the study of metal loading but with different wavelength which was 420 nm. The experiment was run for two hours. Table 4-7 shows the comparison for the NSW analysis for nickel loading catalyst at 365 nm wavelength and 420 nm wavelength.

Table 4-7: NSW analysis for nickel loading catalyst.

Sample	Ph	Conductivity (mS/cm)	TDS (g/L)	BOD (mg/L)	COD (mg/L)
Fresh NSW	8.20	48.8	31.3	33.03	669
365 nm	8.14	46.9	30.5	10.50	100
420 nm	8.16	49.9	31.9	1.5	53

Table 4-7 shows that there is a reduction of Ph, conductivity, TDS, BOD and COD for the analysis using the 365 nm wavelength light. While for the 420 nm wavelength light, there are only reduction for the pH, BOD and COD. For the conductivity and TDS, there are increment in value.

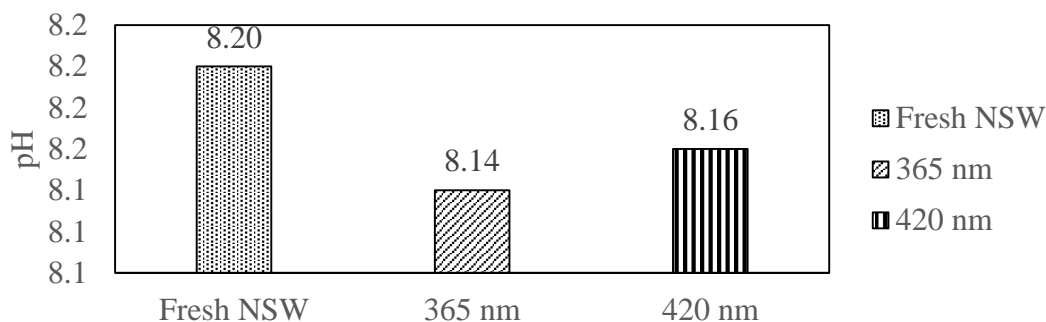


Figure 4-18: NSW analysis for pH.

Figure 4-18 shows the value for the pH for the fresh NSW and the NSW after testing with 365 nm and 420 nm wavelength. While Figure 4-19 show the percentage of reduction for the pH value for the both wavelength light. The initial value for the NSW before the experiment was 8.20. The value then reduce to 8.14 when using the 365 nm wavelength light. These reduction is at 0.73%. While the value of Ph reduce to 8.16 when using the 420 nm wavelength light. The percentage of reduction is at 0.49%.

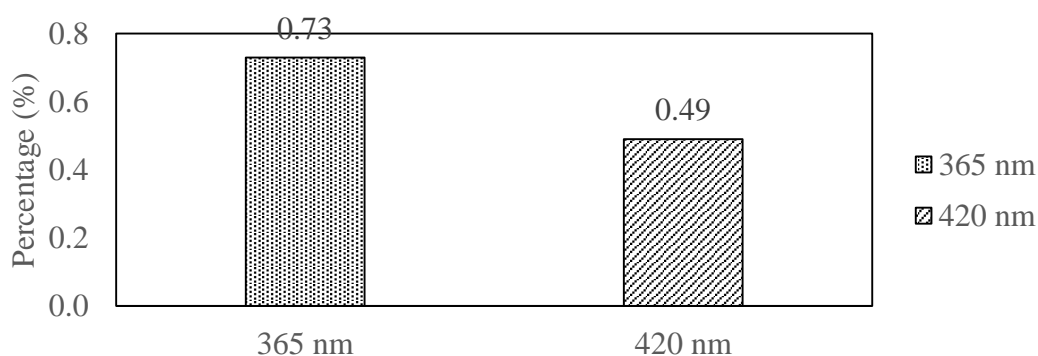


Figure 4-19: Percentage of reduction for pH.

From these data, it is found that the 420 nm wavelength light has the higher reduction of pH compared to the 365 nm wavelength light for the nickel loading catalyst. The percentage of reduction difference between these two are at 0.24%.

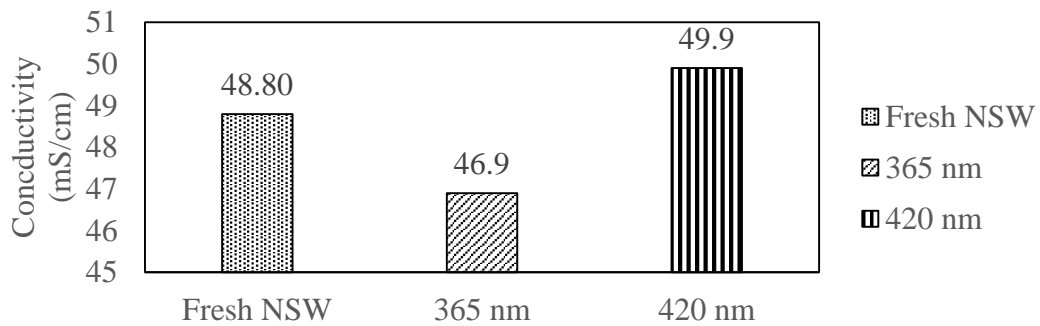


Figure 4-20: NSW analysis for conductivity.

Figure 4-20 shows the value for the conductivity for the fresh NSW and the NSW after testing with 365 nm and 420 nm wavelength. For the conductivity, there is only reduction for the 365 nm wavelength light. While for the 420 nm wavelength light has an increment of value. The 365 nm wavelength light has a reduction of conductivity from 48.8 mS/cm to 46.9 mS/cm. The percentage of reduction is at 3.89 %. For the 420 nm wavelength light, the value for conductivity increase from 48.8 mS/cm to 49.9 mS/cm. The increment percentage was at 2.25%. These increment was due to the domination of distillation process where 50 ml of distillate was produced.

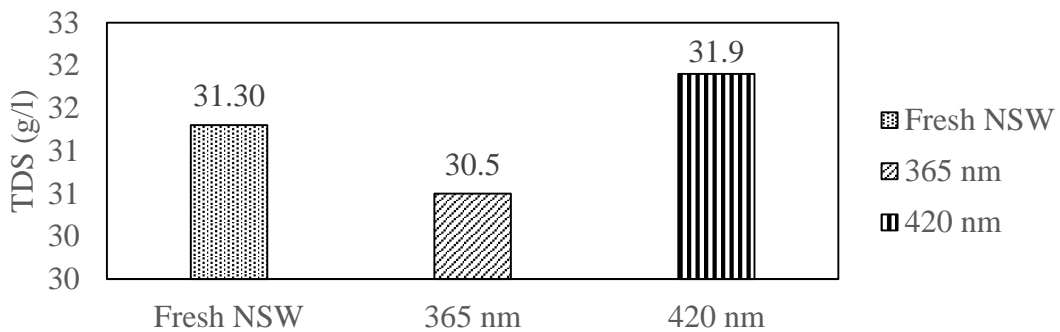


Figure 4-21: NSW analysis for TDS.

Figure 4-21 shows the value for the TDS for the fresh NSW and the NSW after testing with 365 nm and 420 nm wavelength. For the conductivity, there is only reduction for the 365 nm wavelength light. While for the 420 nm wavelength light has an increment of value. The initial value for the TDS is 31.3 g/l. These NSW TDS value decrease to 30.5 g/l for the 365 nm wavelength light. The percentage of reduction is at 2.56%. For the 420 nm wavelength light has an increment to 31.9 g/l. The percentage for the increment is at 1.92%.

From the data obtained for the conductivity and TDS, it can be concluded that the catalyst work best at 365 nm wavelength light where there is reduction for the conductivity and TDS.

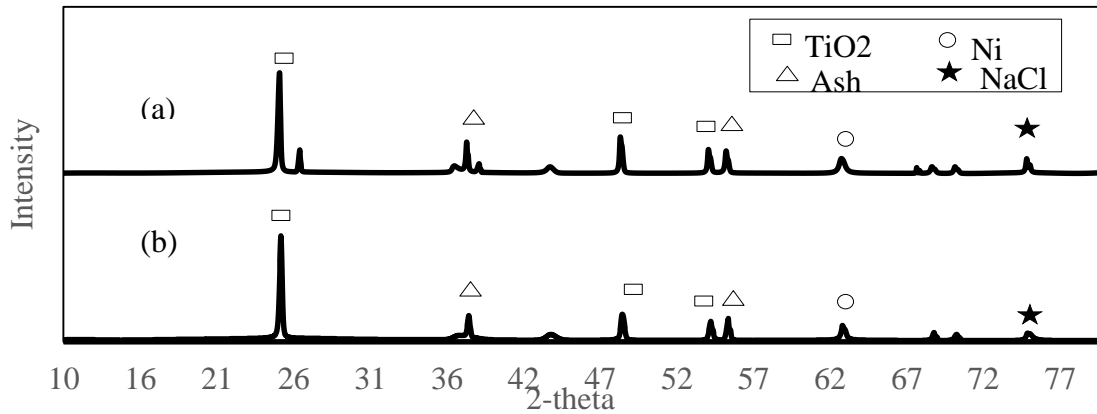


Figure 4-22: XRD analysis (a) 365 nm (b) 420 nm.

The reduction of conductivity and the TDS for the 365 nm wavelength can be proven based the XRD analysis which is illustrated in Figure 4-22. It is found that there is the presence of salt in the XRD analysis. These show that the catalyst has the ability to absorb salt. For the 420 nm wavelength light, even though there is no reduction of conductivity and TDS, there is still absorption of salt. These is proven with the XRD analysis for the 420 nm wavelength light. These is due to the presence of salt in the XRD analysis shown in Figure 4-22.

Table 4-8: BET analysis for no metal loading catalyst

Type of Wavelength	Specific surface area (m <sup>2</sup> /g)		Pore volume x10 <sup>2</sup> (cm <sup>3</sup> /g)		Pore size (nm)	
	Before treatment	After treatment	Before treatment	After treatment	Before treatment	After treatment
365 nm	13.52	16.75	0.34	0.45	1.19	1.11
420 nm	13.52	16.97	0.34	0.47	1.19	1.04

Beside XRD analysis, the reduction of conductivity and TDS can also prove using BET analysis illustrated in Table 4-8. For the 365 nm specific surface area, the area increase

from 13.52 m<sup>2</sup>/g to 16.75 m<sup>2</sup>/g. The increment percentage of the specific surface area is 23.89%. While the 420 nm wavelength light, the increment is from 13.52 m<sup>2</sup>/g to 16.97 m<sup>2</sup>/g which the percentage of increment is at 25.52%.

For the pore volume, the 365 nm wavelength has an increase from 0.0034 cm<sup>3</sup>/g to 0.0045 cm<sup>3</sup>/g which is at 32.35% increase. While for the 420 nm wavelength, the pore volume increase from 0.0034 cm<sup>3</sup>/g to 0.0047 cm<sup>3</sup>/g which is at 8.5% increase 38.24% in size.

For the pore size, the 365 nm has a reduction which is from 1.19 nm to 1.11 nm which is at 6.72% reduction. While the 420 nm has a reduction form 1.19 nm to 1.04 nm which is at 12.6% reduction.

From these it is proven that the catalyst absorb salt due to the increase in specific area and pore volume and the decrease of pore size. From the BET analysis also, it shows that there is an improvement in salt absorption where the specific surface area and pore volume has an increment in area and volume at 420 nm wavelength compared to 365 nm wavelength. There also an increment in reduction of pore size also at 420 nm wavelength.

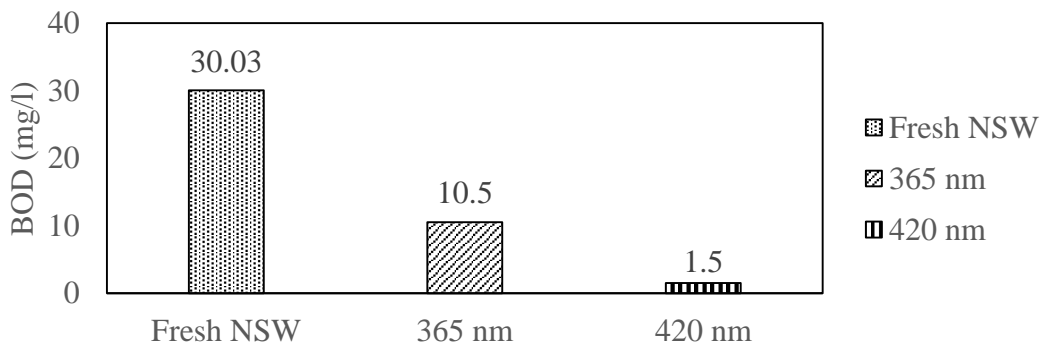


Figure 4-23: NSW analysis for BOD.

Figure 4-23 shows the value of BOD for the 365 nm and 420 nm wavelength light while Figure 4-24 show the percentage of reduction of BOD of the two wavelength. The initial value for the NSW BOD is 30.03 mg/l. These value is reduced to 10.5 mg/l when using the 365 nm wavelength light. The percentage of reduction is at 68.21%. While for the 420 nm wavelength light, the initial value reduce to 1.5 mg/l which is at 95.46% of reduction.

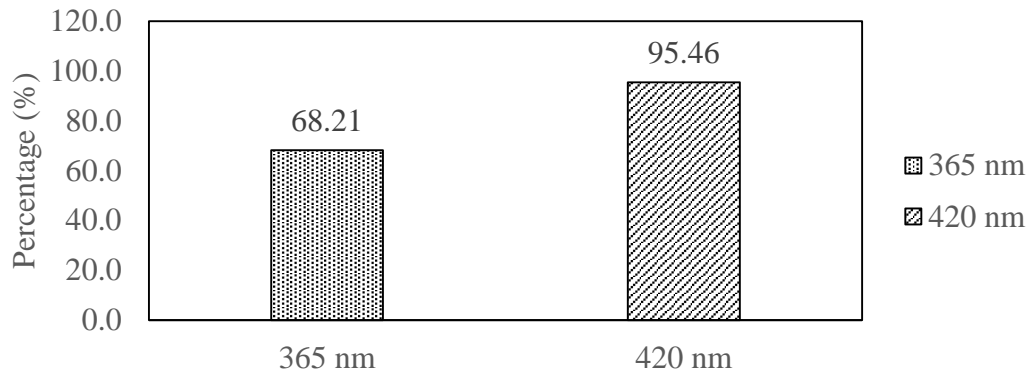


Figure 4-24: Percentage of reduction for BOD.

From these data, it is found that the 420 nm wavelength has the higher BOD reduction compared to the 365 nm wavelength light. The difference of reduction between the two wavelengths is 27.25%. These shows that the nickel loading catalyst has an increase in performance for BOD reduction when 420 nm wavelength light was used.

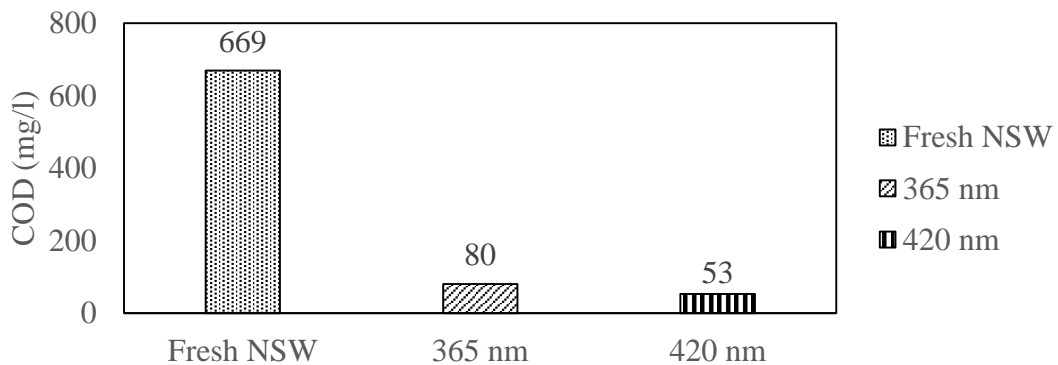


Figure 4-25: NSW analysis for COD.

Figure 4-25 shows the value of COD for the 365 nm and 420 nm wavelength light while Figure 4-26 show the percentage of reduction of COD of the two wavelength. The initial value for the NSW COD is 669 mg/l. The 365 nm wavelength has reduce the initial value of NSW to 80 mg/l which at 88.04% of reduction. While 420 nm wavelength has the ability to reduce the initial value of NSW to 53 mg/l. The percentage of reduction is at 92.08%.

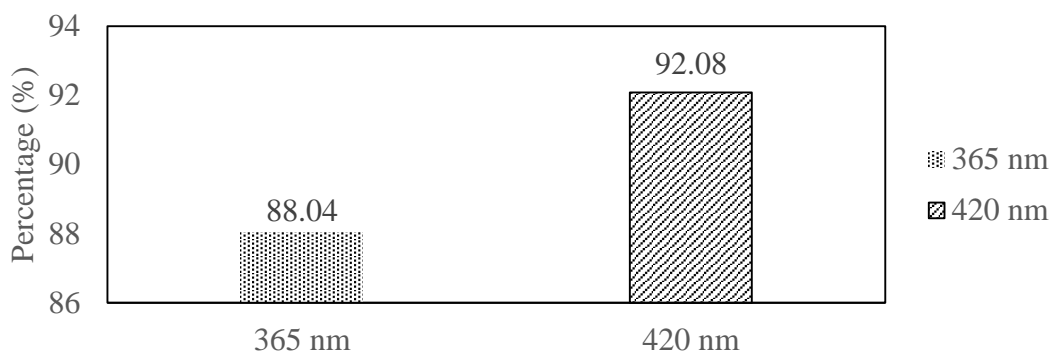


Figure 4-26: Percentage of reduction for COD.

From these two figure, it is found that the nickel loading has higher reduction of COD at 420 nm wavelength light compared to 365 nm wavelength light. These is due to the increase of performance of the reduction of COD.

From all the data obtained for the nickel loading catalyst, it is found that the nickel loading catalyst has an increase of performance at 420 nm wavelength light compared to the 365 nm wavelength light. These was due to the percentage of reduction for the BOD, and COD increases in value when tested at 420 nm wavelength. The BET analysis also help to show that increase of salt absorption due to the increase of specific surface area and the pore volume and the decrease in pore size compared with the 365 nm wavelength. These result also shows that the addition of nickel to the hybrid TiO<sub>2</sub> and biomass ash catalyst help to improve the performance of the catalyst.

#### 4.4.3 Ferum Loading

Ferum loading catalyst is a catalyst that contain TiO<sub>2</sub>, biomass ash, and ferum with the weight ratio of 45:45:10. These catalyst was tested using the same reactor as the study of metal loading but with different wavelength which was 420 nm. The experiment was run for two hours. Table 4-9 shows the comparison for the NSW analysis for ferum loading catalyst at 365 nm wavelength and 420 nm wavelength.

Table 4-9: NSW analysis for nickel loading catalyst.

Sample	Ph	Conductivity (mS/cm)	TDS (g/L)	BOD (mg/L)	COD (mg/L)
Fresh NSW	8.20	48.8	31.3	33.03	669
365 nm	8.40	47.7	30.6	19.26	101
420 nm	8.16	50.1	32.0	0.90	36

Table 4-9 shows that there is a reduction of conductivity, TDS, BOD and COD for the analysis using the 365 nm wavelength light. While for the 420 nm wavelength light, there are only reduction for the pH, BOD and COD. For the conductivity and TDS, there are increment in value.

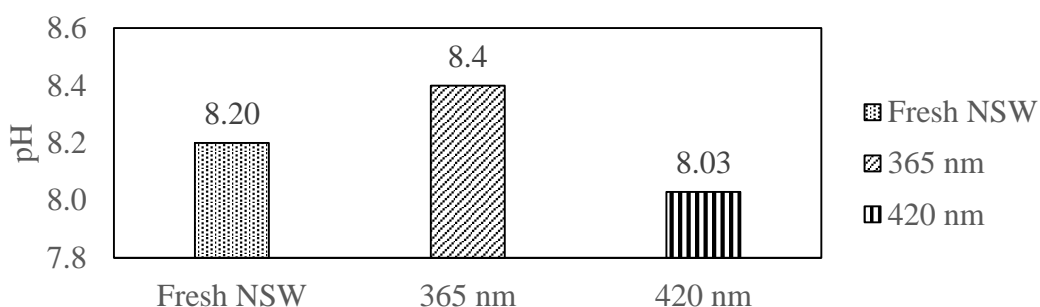


Figure 4-27: NSW analysis for pH.

Figure 4-27 shows the value for the pH for the fresh NSW and the NSW after testing with 365 nm and 420 nm wavelength. The initial value for the NSW before the experiment was 8.20. The value then increase to 8.4 when using the 365 nm wavelength light. These increment is at 2.44%. While the value of Ph reduce to 8.03 when using the 420 nm wavelength light. The percentage of reduction is at 2.07%.

From these data, it is found that the 420 nm wavelength light has the higher reduction of pH compared to the 365 nm wavelength light for the ferum loading catalyst.

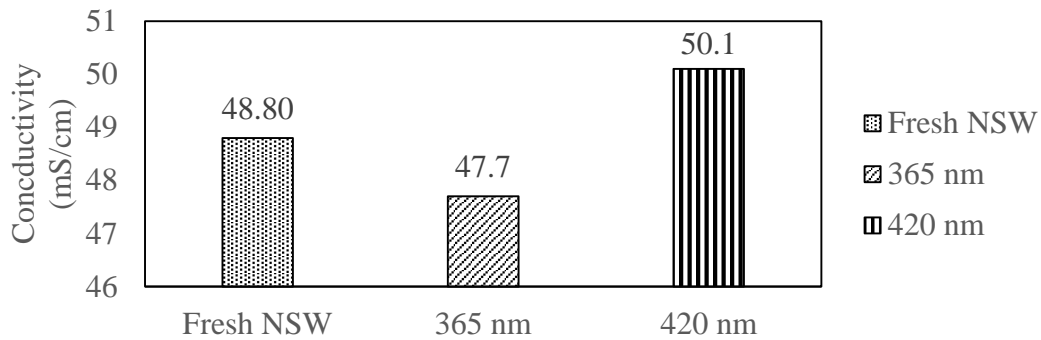


Figure 4-28: NSW analysis for conductivity.

Figure 4-28 shows the value for the conductivity for the fresh NSW and the NSW after testing with 365 nm and 420 nm wavelength. For the conductivity, there is only reduction for the 365 nm wavelength light. While for the 420 nm wavelength light has an increment of value. The 365 nm wavelength light has a reduction of conductivity from 48.8 mS/cm to 47.7 mS/cm. The percentage of reduction is at 2.25 %. For the 420 nm wavelength light, the value for conductivity increase from 48.8 mS/cm to 50.1 mS/cm. The increment percentage was at 2.66%. These increment was due to the domination of distillation process where 50 ml of distillate was produced.

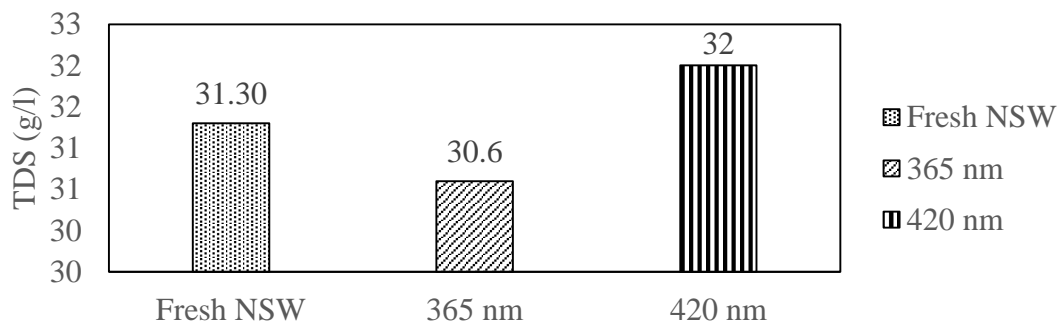


Figure 4-29: NSW analysis for TDS.

Figure 4-29 shows the value for the TDS for the fresh NSW and the NSW after testing with 365 nm and 420 nm wavelength. For the conductivity, there is only reduction for the 365 nm wavelength light. While for the 420 nm wavelength light has an increment of value. The initial value for the TDS is 31.3 g/l. These NSW TDS value decrease to 30.6 g/l for the 365 nm wavelength light. The percentage of reduction is at 2.24%. For the 420 nm wavelength light has an increment to 32 g/l. The percentage for the increment is at 2.24%.

From the data obtained for the conductivity and TDS, it shows that the catalyst work best at 365 nm wavelength light where there is reduction for the conductivity and TDS.

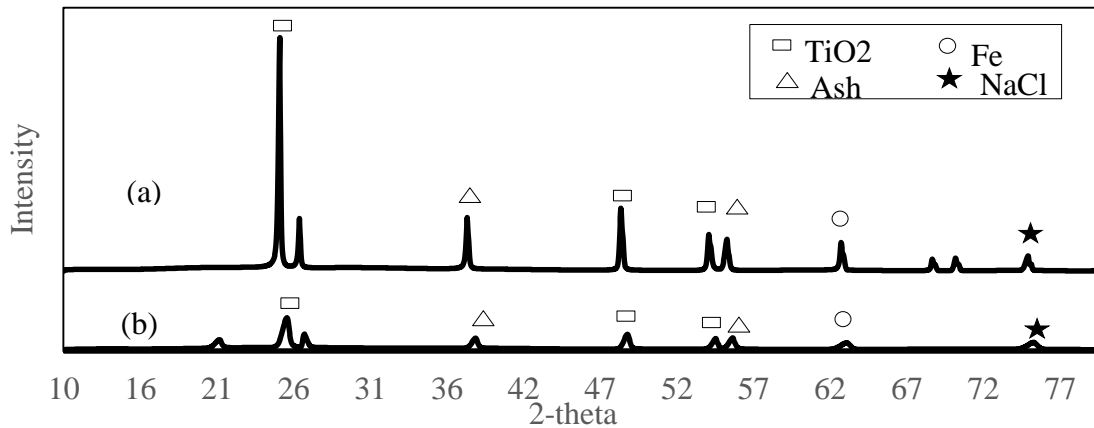


Figure 4-30: XRD analysis (a) 365 nm (b) 420 nm.

The reduction of conductivity and the TDS for the 365 nm wavelength can be proven based the XRD analysis which is illustrated in Figure 4-30. It is found that there is the presence of salt in the XRD analysis. These show that the catalyst has the ability to absorb salt. For the 420 nm wavelength light, even though there is no reduction of conductivity and TDS, there is still absorption of salt. These is proven with the XRD analysis for the 420 nm wavelength light. These is due to the presence of salt in the XRD analysis shown in Figure 4-30.

Table 4-10: BET analysis for ferum loading catalyst

Type of Wavelength	Specific surface area (m <sup>2</sup> /g)		Pore volume x10 <sup>2</sup> (cm <sup>3</sup> /g)		Pore size (nm)	
	Before treatment	After treatment	Before treatment	After treatment	Before treatment	After treatment
365 nm	12.36	13.71	0.28	0.34	1.18	1.11
420 nm	12.36	15.44	0.28	0.47	1.18	1.10

Beside XRD analysis, the reduction of conductivity and TDS can also prove using BET analysis illustrated in Table 4-10. For the 365 nm specific surface area, the area increase from 12.36 m<sup>2</sup>/g to 13.71 m<sup>2</sup>/g. The increment percentage of the specific surface area is 10.92%. While the 420 nm wavelength light, the increment is from 12.36 m<sup>2</sup>/g to 15.44 m<sup>2</sup>/g which the percentage of increment is at 24.92%.

For the pore volume, the 365 nm wavelength has an increase from 0.0028 cm<sup>3</sup>/g to 0.0034 cm<sup>3</sup>/g which is at 21.43% increase. While for the 420 nm wavelength, the pore volume increase from 0.0028 cm<sup>3</sup>/g to 0.0047 cm<sup>3</sup>/g which is at 67.86%.

For the pore size, the 365 nm has a reduction which is from 1.18 nm to 1.11 nm which is at 5.93% reduction. While the 420 nm has a reduction form 1.19 nm to 1.10 nm which is at 6.78% reduction.

From these it is proven that the catalyst absorb salt due to the increase in specific area and pore volume and the decrease of pore size. From the BET analysis also, it shows that there is an improvement in salt absorption where the specific surface area and pore volume has an increment in area and volume at 420 nm wavelength compared to 365 nm wavelength. There also an increment in reduction of pore size also at 420 nm wavelength.

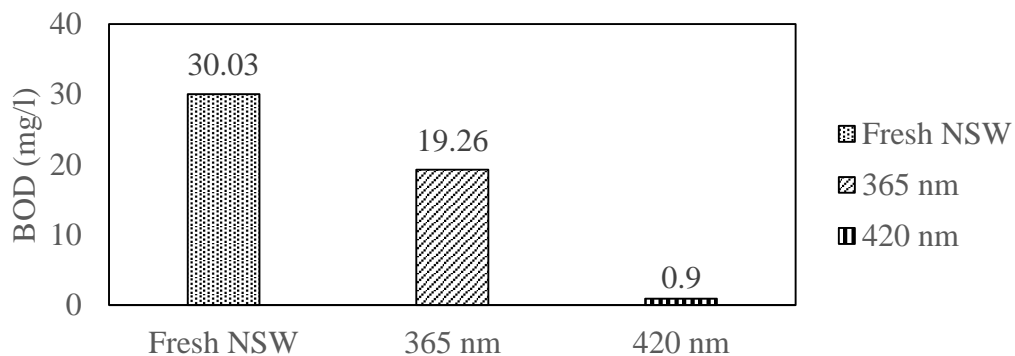


Figure 4-31: NSW analysis for BOD.

Figure 4-31 shows the value of BOD for the 365 nm and 420 nm wavelength light while Figure 4-32 show the percentage of reduction of BOD of the two wavelength. The initial value for the NSW BOD is 30.03 mg/l. These value is reduced to 19.26 mg/l when using the 365 nm wavelength light. The percentage of reduction is at 41.69%. While for the 420 nm wavelength light, the initial value reduce to 0.9 mg/l which is at 97.28% of reduction.

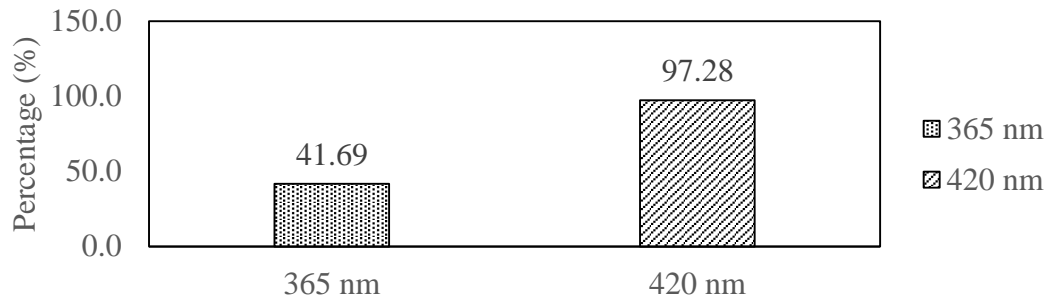


Figure 4-32: Percentage of reduction for BOD.

From these data, it is found that the 420 nm wavelength has the higher BOD reduction compared to the 365 nm wavelength light. The difference of reduction between the two wavelengths is 55.59%. These shows that the ferum loading catalyst has an large increase in performance for BOD reduction when 420 nm wavelength light was used.

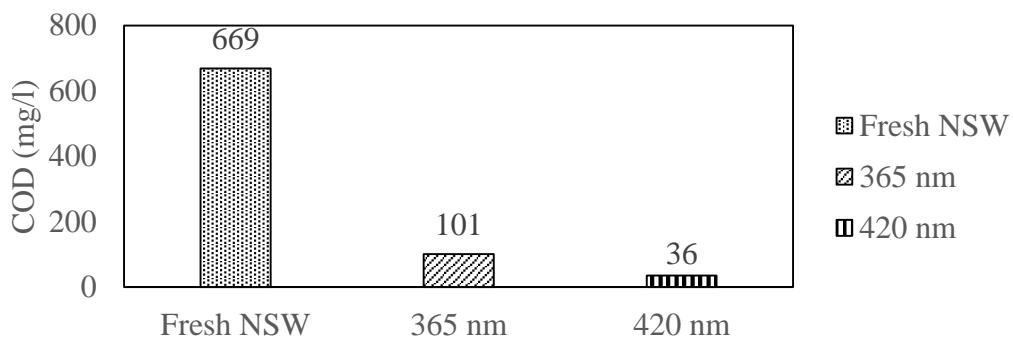


Figure 4-33: NSW analysis for COD.

Figure 4-33 shows the value of COD for the 365 nm and 420 nm wavelength light while Figure 4-34 show the percentage of reduction of COD of the two wavelength. The initial value for the NSW COD is 669 mg/l. The 365 nm wavelength has reduce the initial value of NSW to 101 mg/l which at 84.9% of reduction. While 420 nm wavelength has the ability to reduce the initial value of NSW to 36 mg/l. The percentage of reduction is at 94.62%.

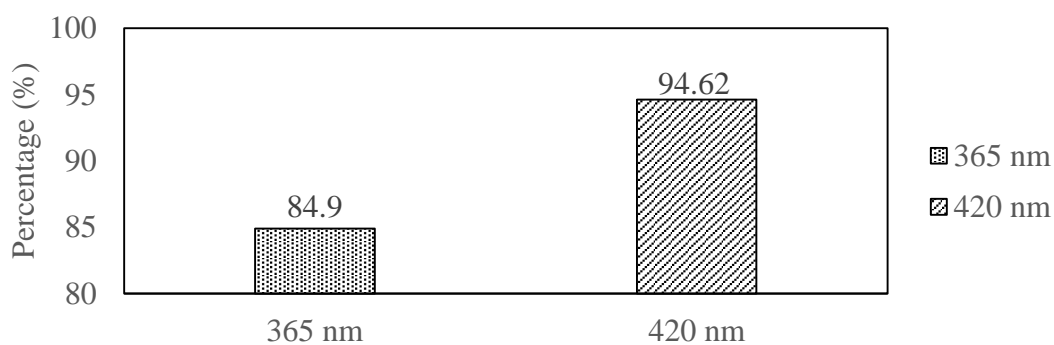


Figure 4-34: Percentage of reduction for COD.

From these two figure, it is found that the ferum loading has higher reduction of COD at 420 nm wavelength light compared to 365 nm wavelength light. These is due to the increase of performance of the reduction of COD.

From all the data obtained for the ferum loading catalyst, it is found that the nickel loading catalyst has an increase of performance at 420 nm wavelength light compared to the 365 nm wavelength light. These was due to the percentage of reduction for the BOD, and COD increases drastically in value when tested at 420 nm wavelength. The BET analysis also help to show that increase of salt absorption due to the increase of specific surface area and the pore volume and the decrease in pore size compared with the 365 nm wavelength. These result also shows that the addition of ferum to the hybrid TiO<sub>2</sub> and biomass ash catalyst help to improve the performance of the catalyst.

#### 4.4.4 SEM Characterization

The three catalyst which are no metal loading, nickel loading and ferum loading catalyst also characterize using the SEM to see the morphology of the catalyst before and after the experiment. Figure 4-35 shows the SEM image for the 420 nm wavelength light.

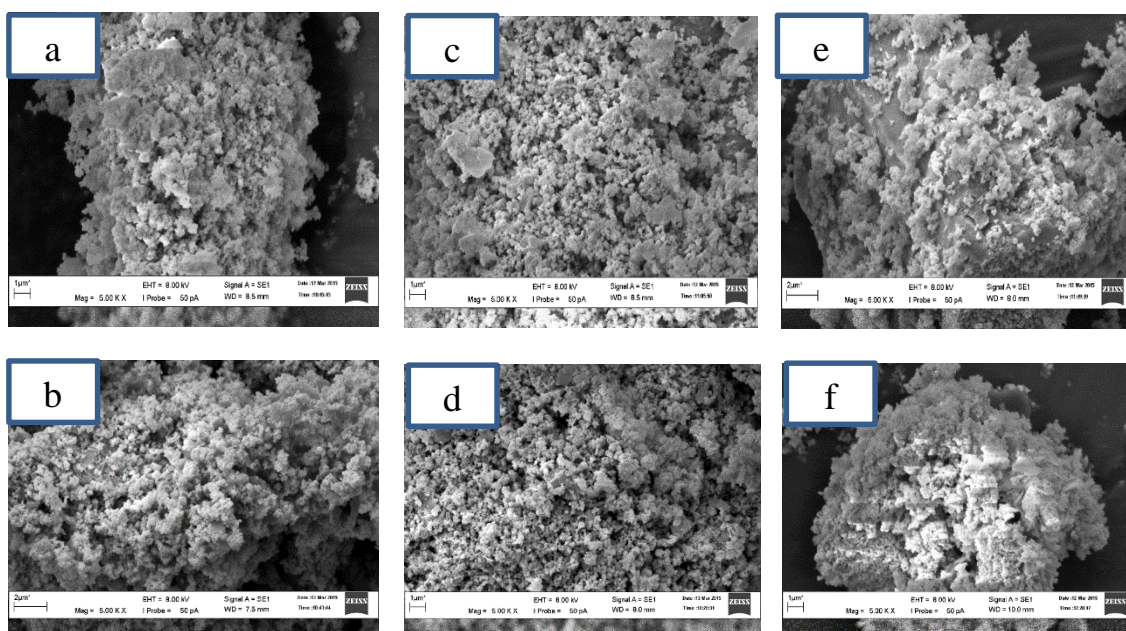


Figure 4-35: SEM image of the used catalyst: (a) fresh no metal loading (b) used no metal loading (c) fresh nickel loading (d) used nickel loading (e) fresh ferum loading (f) used ferum loading

The SEM image of the catalyst before and after the experiment show that the structure is not ruptured and there is an increase crystalline structure on the surface of the catalyst which might be salt attach at the surface of the catalyst after the experiment. Because the structure of the catalyst do not rupture, further analysis should be done to investigate the durability of the catalyst.

#### 4.4.5 Summary

Figure 4-36 shows the comparison of the percentage of reduction of the 365 nm and 420 nm wavelength light. From the graph, it shows that there is no reduction for the 420 nm wavelength for the parameter of conductivity and TDS. These is due to the domination of distillation process that occur during the experiment which was cause due to the increase of temperature to 100 °C. The temperature increase because the 420 nm wavelength light generated high heat compared to 365 nm wavelength light. For the 365 nm, there is reduction in conductivity and TDS for the three catalyst and nickel has the higher

reduction compared to the two catalyst and it is proven through the BET analysis where nickel has the highest increase in specific surface area and pore volume. For the BOD and COD, nickel loading catalyst also has the highest reduction compared to the two at 365 nm.

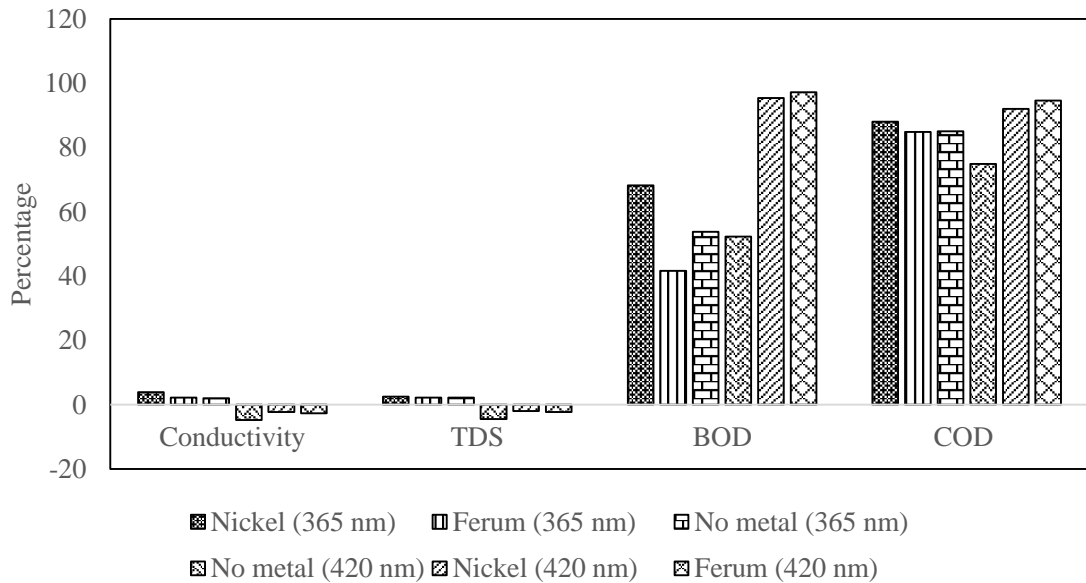


Figure 4-36 : The overall comparison for the percentage of reduction for 365 nm and 420 nm wavelength light.

The reduction of BOD and COD at 420 nm, ferum loading has the highest reduction and ferum show drastic improvement compared to the other two catalyst. Nickel also has improvement in the reduction of BOD and COD. For the no metal loading catalyst, the reduction percentage has decrease. These might due to the metal band gap characterization of the no metal is not suitable reacting at 420 nm wavelength. From the figure also, it can be concluded that nickel work best at 365 nm wavelength because nickel has the highest overall reduction while ferum work best at 420 nm because there is a drastic increase in performance. Besides that, ferum also has the highest reduction for BOD and COD for 420 nm wavelength. The different performance at different wavelength due to the different of band gap of the metal where ferum has smaller band gap than nickel.

## 5 CONCLUSION AND RECOMMENDATION

### 5.1 Conclusion

The objective of these research were achieved which were to study the effectiveness of metal loading with hybrid TiO<sub>2</sub> and biomass ash catalyst in photocatalytic reaction and to study the effect of wavelength in the photocatalytic reaction. In these research, wet impregnation method was used to prepare the catalyst. After the catalyst was prepared, the catalyst was used for photocatalytic reaction with NSW. The NSW was analyzed before and after the photocatalytic reaction.

From the analysis, it was found that the no metal loading catalyst reduction for conductivity of the NSW using 365 nm wavelength light was at 2.05%, TDS at 2.24%, BOD at 53.77% and COD at 85.05%. While for the nickel catalyst, the reduction for the conductivity was at 3.89%, TDS at 2.56%, BOD at 68.21% and COD 88.04%. For the ferum loading catalyst, the reduction of conductivity was at 2.25%, TDS at 2.56%, BOD at 41.69% and COD at 84.9%. For the 420 nm wavelength light, the conductivity and the TDS value increases due to the domination of distillation process. The 420 nm wavelength light also has the ability to rise up the seawater temperature up to 100 °C which help in the domination of the distillation. Therefore, there were only reduction in BOD and COD. The reduction of BOD for no metal loading catalyst was at 52.32% and COD at 74.89%. For the nickel loading catalyst, the reduction of BOD was at 95.46% and COD at 92.08%. While for the ferum loading catalyst, the reduction of BOD was at 97.28% and COD at 94.62%.

From the data, it is found that nickel loading catalyst performed best at photocatalytic reaction using 365 nm wavelength light. The nickel loading catalyst, has the overall highest reduction compared to no metal loading and ferum loading catalyst. While at photocatalytic reaction using 420 nm wavelength light, ferum loading catalyst has the best overall reduction compared to nickel loading and no metal loading catalyst. The difference performance was because of the performance of the metal loading was due to the different characterization of the metal band gap in which the smaller the band gap required bigger wavelength. Nickel has bigger band gap than ferum. From these, it can be concluded that the addition of metal loading to hybrid TiO<sub>2</sub> and biomass ash catalyst

improve the performance catalyst and metal loading catalyst performance at difference wavelength light depend on the metal band gap characteristic.

## **5.2 Recommendation**

In order to improve the research, there are several aspects should be remarked. The recommendation are:

- Test the durability of the catalyst so that the lifetime of the catalyst can be determined.
- Improve the ability of the catalyst so that it can be used at natural light source.
- Design and build the photocatalytic reactor in pilot scale.
- Test the effectiveness of the catalyst and photocatalytic reaction on industrial waste water.

## References

- A. Fujishima, K. H. T. W., 1999. TiO<sub>2</sub> Photocatalysis: Fundamentals and Applications. *BKC*.
- Akili, D. K., Ibrahim, K. K. & Jong-Min, W., 2008. Advances in Seawater Desalination Technologies. *Journal of Desalination*, pp. 47-69.
- Anon., 2004. [Online]  
Available at: <http://www.deltawerken.com/What-is-water/341.html>
- Anon., 2014. *Oxford Press*. [Online]  
Available at: <http://www.oxforddictionaries.com/definition/english/water>
- Anon., 2014. *USGS*. [Online]  
Available at: <http://water.usgs.gov/edu/drinkseawater.html>
- Bard, A. J., 1979. Photoelectrochemistry and Heterogeneous Photocatalysis at Semiconductors. *J. Photochem*, p. 59–75.
- Burda, C. L. Y. C. X. S. A. S. J. G. J., 2003. Enhanced nitrogen doping in TiO<sub>2</sub> nanoparticles. *Nano Lett.* 3, p. 1049–1051.
- Chang, C.Y.; Wu, N.L., 2010. Process analysis on photocatalyzed dye decomposition for water treatment with TiO<sub>2</sub>-coated rotating disk reactor. *Ind. Eng. Chem. Res.*, 49, 12173–12179.
- Chen, D. R. A., 1999. Photocatalytic kinetics of phenol and its derivatives over UV irradiated TiO<sub>2</sub>. *Appl. Catal.*, p. 143–157.
- Chiou, C.-H. W. C.-Y. J. R.-S., 2008. Photocatalytic degradation of phenol and m-nitrophenol using irradiated TiO<sub>2</sub> in aqueous solutions. *Sep. Purif. Technol.* 62, p. 559–564.
- Chong, M. N., 2010. Recent Development in Photocatalytic Water Treatment Technology: A review. *Water Research*, pp. 2997-3027.
- Demeestere, K., Dewulf, J., Ohno, T., Salgado, P.H., Van Langenhove, H., 2005. Visible light mediated photocatalytic degradation of gaseous trichloroethylene and dimethyl sulfide on modified titanium dioxide. *Appl. Catal. B* 61,, p. 140–149.
- Esplugas, S. et al., 2002. Comparison of Different Advanced Oxidation Process for Phenol Degradation. *Water Res.* 36, pp. 1034-1042.
- Francois, V., Francois, M., Emmanuelle, A. & Philippe, B., 2008. Multi-objective Optimization of RO Desalination Plants. *Journal of Desalination*, pp. 96-118.

- Fujishima, A., 2005. Titanium dioxide photocatalysis: present situation and future approaches. *C. R. Chimie* 9, p. 751.
- Fujishima, A. H., 1972. Electrochemical photolysis of water at a semiconductor electrode. *Nature*, p. 37–38.
- Fujishima, A., Rao, T. N. & Tryk, D. A., 1995. *J. Photochem. Photobiol.*
- Ghaffour, N., Reddy, V. K. & Abu-Arabi, M., 2011. Technology Development and Application of Solar Energy in Desalination: MERDC Contribution. *Journal of Renewable and Sustainable Energy Reveiw* 15, pp. 4410-4415.
- Gleick, P. H., 1996. *Water Resources in Encyclopedia of Climate and Weather, vol. 2.* New York: University Press.
- Greenlee, L. F. D. F. L. B. D. F. B. M., 2009. Reverse osmosis desalination: Water sources, technology,. *Water Research*, p. 2318.
- Ji, Z.X.; Callahan, D.M.; Ismail, M.N.; Warzywoda, J.; Sacco, A. 2011. Development and characterization of a titanosilicate ETS-10-coated optical fiber reactor towards the photodegradation of methylene blue. *J. Photochem. Photobiol. A*, 217, 22–28.
- Khan, S. A. J., 1999. Photoelectrochemical splitting of water at nanocrystalline n-Fe<sub>2</sub>O<sub>3</sub> thin-film electrodes. *J. Phys. Chem.*, p. 7184–7189.
- Kim, M.J.; Choo, K.H.; Park, H.S., 2010. Photocatalytic degradation of seawater organic matter using a submerged membrane reactor. *J. Photochem. Photobiol. A*, 216, 215–220.
- Lee, Y. et al., 2007. M. Zinc Germanium Oxynitride as a Photocatalyst for Overall Water Splitting under Visible Light. *J. Phys. Chem. C*, p. 1042–1048.
- Lokiec, F., 2003. South Israel 100 million m<sup>3</sup>/y seawater desalination. *Desalination*, p. 29.
- Maeda, K. et al., 2005. K. GaN:ZnO Solid Solution as a Photocatalyst for Visible-Light-Driven Overall Water Splitting. *J. Am. Chem. Soc*, p. 8286–8287.
- Magalhães, A. N. D. R.-D. P. D. S. E., 2004. Catalytic activity of porous TiO<sub>2</sub> obtained by sol–gel process in the degradation of phenol. *J. Non-Cryst. Solids*, p. 185–189.
- Malato, S. et al., 2009. Decontamination and Disinfection of Water With Soalr Collectors. *Ctal.Today*, pp. 147,1-59.
- Mohamed, R. I. A. O. I. I. I., 2005. Preparation of TiO<sub>2</sub>-ZSM-5 zeolite for photodegradation of EDTA. *Mol. Catal. A* 238, p. 151–157.
- Mohaputra, S. M. M. M. V., 2007. *J Phys. Chem.*, p. 8677–8685.

Natarajan, T.S.; Thomas, M.; Natarajan, K.; Bajaj, H.C.; Tayade, R.J., 2011. Study on UV-LED/TiO<sub>2</sub> process for degradation of rhodamine B dye. *Chem. Eng. J.*, 169, 126–134.

Nickels, P.; Zhou, H.; Basahel, S.N.; Obaid, A.Y.; Ali, T.T.; Al-Ghamdi, A.A.; El-Mossalamy, E.-S.H.; Ayoubi, A.O.; Lynch, S.A., 2012. Laboratory scale water circuit including a photocatalytic reactor and a portable in-stream sensor to monitor pollutant degradation. *Ind. Eng. Chem. Res.*, 51, 3301–3308.

Oppenlander, T., 2003. *Photochemical Purification of Water and Air*. Wiley-VCH.

Park, H. C. W., 2005. Photocatalytic reactivities of nafion-coated TiO<sub>2</sub> for the degradation of charged organic compounds under UV or Visible light. *J. Phys. Chem. B*, p. 11667–11674.

Parsons, S., 2004. *Advanced Oxidation Processes for Water and Wastewater Treatment*. Cornwall, UK: IWA Publishing.

Pereira, J.; Vilar, V.J.P.; Borges, M.T.; Gonzalez, O.; Esplugas, S.; Boaventura, R.A.R., 2011. Photocatalytic degradation of oxytetracycline using TiO<sub>2</sub> under natural and simulated solar radiation. *Sol. Energy*, 85, 2732–2740.

Pera-Titus, M. et al., 2004. Degradation of Chlorophenols by Means of Advanced Oxidation Process: A general Review. pp. 219-256.

Rao, N.N.; Chaturvedi, V.; Puma, G.L., 2012. Novel pebble bed photocatalytic reactor for solar treatment of textile wastewater. *Chem. Eng. J.*, 184, 90–97.

Service, R., 2006. Desalination freshen up. *Science* 313, pp. 1088-109.

Shkhashiri, 2011. *Chemical of The week: Water for General Chemistry*. [Online] Available at: [www.scifun.org](http://www.scifun.org)

Suryaman, D.; Hasegawa, K.; Kagaya, S.; Yoshimura, T., 2009. Continuous flow photocatalytic treatment integrated with separation of titanium dioxide on the removal of phenol in tap water. *J. Hazard. Mater.*, 171, 318–322

Vilar, V.J.P.; Maldonado, M.I.; Oller, I.; Malato, S.; Boaventura, R.A.R., 2009. Solar treatment of cork boiling and bleaching wastewaters in a pilot plant. *Water Res.*, 43, 4050–4062.

Wang, X.P.; Lim, T.T., 2010. Solvothermal synthesis of C-N codoped TiO<sub>2</sub> and photocatalytic evaluation for bisphenol a degradation using a visible-light irradiated led photoreactor. *Appl.Catal. B*, 100, 355–364.

Wolf, A., 1999. *Water and Human Security. AVISO: An Information Bulletin on Global Environmental Change and Human Security*.

- Xiang Zheng, D. C. ., Q. W. ., Z. Z., 2013. Seawater desalination in China: Retrospect and prospect. *Chemical Engineering Journal*, p. 404.
- Xu, C. K. R. G. M. K. S., 2006. Photocatalytic effect of carbon modified n-TiO<sub>2</sub> nanoparticles under visible light illumination. *Appl. Catal. B* 64, p. 312–317.
- Zhang, G.; Choi, W.; Kim, S.H.; Hong, S.B., 2011. Selective photocatalytic degradation of aquatic pollutants by titania encapsulated into FAU-type zeolites. *J. Hazard. Mater.* , 188, 198–205.

## APPENDICES

Based on the weight ratio 45% of TiO<sub>2</sub>, 45% of Oil palm fiber ash and 10% of metal loading. This calculation is for the preparation of 10 gram of catalyst.

i) 45 % Oil palm fiber ash

$$\text{Weight of fiber ash} = \frac{45}{100} \times 10 \text{ gram} = 4.5\text{gram}$$

ii) 45% of TiO<sub>2</sub>

$$\frac{45}{100} \times 10 = 4.5 \text{ gram}$$

$$\frac{47.867 \text{ Ti}}{79.866 \text{ TiO}_2} = \frac{4.5}{x}$$

$$x = 7.51 \text{ gram}$$

Purity 99%

$$\frac{7.51 \text{ gram}}{0.99} = 7.586 \text{ gram}$$

Weight of TiO<sub>2</sub> = 7.586 gram

iii) 10% of metal loading

<p>Nickel Nitrate Hexahydrate</p> $\frac{10}{100} \times 10 \text{ gram} = 1 \text{ gram}$ $\frac{58.69 \text{ Ni}}{290.79 \text{ Ni(NO}_3)_2} = \frac{1}{X}$ <p>X = 4.95 gram</p> <p>Purity 99%</p> $\frac{4.95 \text{ gram}}{0.99} = 5 \text{ gram}$ <p>Weight of Ni(NO<sub>3</sub>)<sub>2</sub> = 5gram</p>	<p>Ferum Nitrate Hydrate</p> $\frac{10}{100} \times 10 \text{ gram} = 1 \text{ gram}$ $\frac{55.845 \text{ Fe}}{404.4 \text{ Fe(NO}_3)_3} = \frac{1}{X}$ <p>X = 7.24 gram</p> <p>Purity 99%</p> $\frac{7.24 \text{ gram}}{0.99} = 7.313 \text{ gram}$ <p>Weight of Fe(NO<sub>3</sub>)<sub>3</sub> = 7.313 gram</p>
--	--